

Phase Transitions and Baryogenesis From Decays

Brian Shuve^{a1} and Carlos Tamarit^{b2}

^aSLAC National Accelerator Laboratory, Menlo Park, CA 94025, USA.

^bInstitute for Particle Physics Phenomenology, Durham University, DH1 3LE, United Kingdom.

Abstract

We study scenarios in which the baryon asymmetry is generated from the decay of a particle whose mass originates from the spontaneous breakdown of a symmetry. This is realized in many models, including low-scale leptogenesis and theories with classical scale invariance. Symmetry breaking in the early universe proceeds through a phase transition that gives the parent particle a time-dependent mass, which provides an additional departure from thermal equilibrium that could modify the efficiency of baryogenesis from out-of-equilibrium decays. We characterize the effects of various types of phase transitions and show that an enhancement in the baryon asymmetry from decays is possible if the phase transition is of the second order, although such models are typically fine-tuned. We also stress the role of new annihilation modes that deplete the parent particle abundance in models realizing such a phase transition, reducing the efficacy of baryogenesis. A proper treatment of baryogenesis in such models therefore requires the inclusion of the effects we study in this paper.

¹E-mail:bshuve@slac.stanford.edu

²E-mail:carlos.tamarit@durham.ac.uk

Contents

1	Introduction	1
2	Review of Asymmetry Generation from Decays	3
3	Asymmetry Generation with a Phase Transition	7
3.1	Time-Dependent Majorana Mass	7
3.2	First-Order Phase Transition	8
3.3	Second-Order Phase Transition	10
3.4	Slowly evolving scalar field	14
4	Asymmetry Damping from New Annihilation Modes	15
4.1	Boltzmann Equations with Annihilations	17
4.2	Analytic Estimate of Annihilation Rates	18
4.3	Numerical Analysis	19
5	Realistic Phase Transitions and Baryogenesis	21
5.1	Single-Field Models	22
5.2	Two-Field Models	24
6	Conclusions	28
A	<i>CP</i>-Violating Source in the Resonant Regime	28
B	Thermally Averaged Rates	29
C	Effective Potential at Zero and Finite Temperature	30
C.1	Single-Field Model	31
C.2	Two-Field (N_I - φ -Majoron) Model	31
D	Annihilation Cross Sections	33
D.1	Broken phase	33
D.2	Unbroken phase	34
E	Select Yukawa Matrices Used in Calculations	34

1 Introduction

The Standard Model (SM) contains many fields but only one dimensionful parameter, since the symmetries of the theory forbid all such terms apart from the Higgs field mass. Consequently, the quarks, leptons, and gauge bosons only acquire masses via interactions with the Higgs field after electroweak symmetry breaking [1, 2, 3]. This property of the SM was confirmed by electroweak precision studies at LEP and SLD [4, 5], as well as the recent discovery of the Higgs boson at the LHC [6, 7].

One implication of the origin of masses in the SM is that field-dependent masses were different in the early universe than today. Finite-temperature corrections to the Higgs potential confine the Higgs field to the origin at early times, and the Higgs field evolved to its present minimum via a phase transition once the universe cooled to a sufficient degree [8, 9, 10]. The time dependence of particle masses provide an “arrow of time” that gives a departure from equilibrium in the early universe beyond the usual Hubble expansion, and this can have profound effects on cosmology.

A departure from equilibrium is crucial to understanding one of the most important unsolved mysteries of particle physics: the origin of the baryon asymmetry. In the absence of an excess of baryons over antibaryons,

most of the protons and neutrons would have annihilated away in the early universe, which is in clear contradiction with the observed abundance of visible matter today. The generation of a baryon asymmetry requires, among other factors, a departure from equilibrium [11]: the processes that create a baryon asymmetry can also destroy it when occurring in reverse and the rates exactly balance when in equilibrium, resulting in a vanishing asymmetry. The electroweak phase transition provides such a departure from equilibrium because baryon-number-violating sphaleron processes are rapid at high temperatures and slow considerably in the broken phase, resulting in electroweak baryogenesis [12, 13, 14]. While the electroweak phase transition in the SM does not occur quickly enough to generate the observed baryon asymmetry [15, 16], extensions of the SM can modify the phase transition and make electroweak baryogenesis a viable theory (for a recent review of electroweak baryogenesis, see [17]).

The baryon asymmetry can also be generated through other mechanisms, the most widely studied of which is baryogenesis through the out-of-equilibrium decay of a massive particle [18]. A heavy self-conjugate field decays into both baryons and antibaryons: CP violation can allow it to decay more frequently into baryons relative to antibaryons, generating an asymmetry. Inverse decay processes destroy the asymmetry but are Boltzmann-suppressed for temperatures $T \ll M$, falling below the expansion rate of the universe and giving a departure from equilibrium. Popular implementations of this mechanism include leptogenesis [19], which is motivated by the see-saw mechanism for generating neutrino masses [20], and Grand-Unified-Theory baryogenesis [21, 22]. In both of these examples, the masses of the particles responsible for baryogenesis are technically natural and could arise from the spontaneous breaking of a symmetry. This is even more motivated in low-scale models where new particle masses are expected to arise dynamically, including models with classical scale invariance [23], or weak-scale models of leptogenesis and neutrino masses [24, 25, 26, 27]. By analogy with the SM, this would give the decaying particles a time-dependent mass in the early universe; indeed, the phase transition typically occurs when $T \sim M$, which is the crucial era for the generation of the baryon asymmetry. In nearly all existing studies of baryogenesis in such models, however, the mass is assumed to have its zero-temperature value throughout the cosmological evolution.

The goal of this paper is to study how baryogenesis via out-of-equilibrium decays is affected by a phase transition that changes the mass of the parent particle. In particular, we are interested in determining whether the additional departure from equilibrium during the phase transition might give rise to an enhancement of the resulting asymmetry. This is feasible in principle: consider an illustrative example with a baryogenesis parent X with zero-temperature mass M_X . In the conventional case where X has constant mass (apart from possible thermal corrections), the asymmetry from early X decays is destroyed by inverse washout processes. Asymmetry generation is only efficient for decays that occur at temperatures $T \ll M_X$ when inverse decays become Boltzmann suppressed and ineffective; however, the number density of X is exponentially suppressed at this time, resulting in a small asymmetry. Let us contrast this with a scenario in which the X mass suddenly turns on due to a phase transition at some temperature $T_c \ll M$: baryon destruction from inverse decays are completely ineffective, while the abundance of X may not have time to relax to its equilibrium value during the phase transition and has an abundance equal to that of a massless field. Since all X decays after the phase transition efficiently generate an asymmetry, this leads to the generation of a much larger asymmetry than with a time-independent M_X .

As we demonstrate in our paper, however, there are several physical effects that complicate the above naïve argument. First, in realistic models where the parent particle in baryogenesis acquires a mass through a phase transition, new couplings are introduced to the fields responsible for symmetry breaking. As we show, a common feature in models with a significant departure from equilibrium is the existence of a light degree of freedom in the accompanying scalar sector. Couplings to the fields responsible for symmetry breaking therefore opens a new mode for the scattering of the heavy particle, which in turn affects the efficiency of baryogenesis. The effects of this damping of the asymmetry have been explored in the case of a time-independent parent mass [28, 29]; we review these effects and study them in combination with a dynamical parent mass.

Secondly, the abundance of X remains constant at the phase transition only if it is of the second order. In contrast, during a first-order phase transition most X are reflected at the phase interface (bubble wall) in the limit $T_c \ll M_X$, limiting the possible generation of a baryon asymmetry. Realizing the condition $T_c \ll M_X$ for a second-order phase transition, as is necessary for the enhancement of the asymmetry, is not a generic feature of realistic models and it is challenging to find models that realize this hierarchy. This is due to

radiative corrections in the symmetry-breaking scalar effective potential, which tend to spoil the properties of the phase transition in the regime in which the parametric enhancement of the asymmetry is realized at leading order. Models in which this enhancement may be consistently realized must involve extra fields with carefully adjusted couplings, and the potential shape required to give a parametric enhancement to the asymmetry requires a relationship among parameters in the theory that lies beyond the level of precision of a full one-loop calculation.

There are not many studies in the literature on the effects of a dynamical parent particle mass on decay baryogenesis. To the best of our knowledge, the earliest studies were in the context of left-right symmetric models in which the particle responsible for lepton-number breaking (the Majoron) undergoes a strong first-order phase transition [30]. However, an asymmetry in such a mechanism actually arises via CP -violating scalar dynamics generating a chemical potential for sphaleron transitions as in Ref. [31], as opposed to a substantial asymmetry from parent decays. For models with a very strong first-order Majoron transition, we argue that asymmetry generation through decays actually becomes hindered by an exponential suppression of the abundance due to reflection of the parent particle at the bubble wall. There has also been a discussion of baryogenesis from decays in quintessence models of dark energy [32], although the evolution of the dynamical masses is so slow in this scenario that no sizeable change in the asymmetry is expected due to the dynamics of the underlying scalar field. Finally, Ref. [27] considered the scenario where the right-handed neutrino responsible for leptogenesis acquire a mass coincident with the electroweak phase transition. In this case, the challenge is in generating an asymmetry before the sphalerons that couple baryon and lepton number become ineffective in the electroweak vacuum. Consequently, their results are sensitive to the time-dependence of sphaleron rates and SM gauge boson masses in a manner that is not amenable to generalization.

Additionally, the aforementioned works did not take into account the effects of Majoron scattering modes on the lepton asymmetry, whose importance was recognized in [28, 29]; these works, however, did not address the effect of time-dependence in the masses of the heavy neutrinos. Outside of the realm of leptogenesis from decays, other studies of cosmological implications of dynamical masses have examined, for example, leptogenesis from interactions with the bubble wall of a first-order CP -violating phase transition [33], leptogenesis in a manner akin to electroweak baryogenesis [34, 35, 36], leptogenesis from the non-thermal production of right-handed neutrinos in bubble-wall collisions [37], as well as the effects of a phase transition on dark matter [38] and on cosmological implications of flavour models [39]. Common to these studies, as well as our own, is the fact that the properties of particles can be very different in the early universe from the present day, and care should be exercised in interpreting and motivating experimental particle searches for such phenomena.

Our study is organized as follows: in Sec. 2, we review out-of-equilibrium-decay baryogenesis in the absence of a phase transition, and in Sec. 3 we derive the dependence of the asymmetry on a time-dependent mass in a toy example. We consider the effects on the asymmetry of couplings between the symmetry-breaking sector and the parent particle in Sec. 4. In Sec. 5 we examine realistic models for phase transitions and the extent to which the phase transitions studied in earlier sections can be achieved, and we conclude with a summary and discussion of our results.

2 Review of Asymmetry Generation from Decays

In this section, we review the mechanism for generating an asymmetry from the out-of-equilibrium decay of a massive particle with time-independent mass [18]. We highlight the dependence of the final baryon asymmetry on the parameters of the model, as this will facilitate a physical understanding of the asymmetry generated in our new model with a phase transition.

Since we ultimately wish to study the decay of a particle whose mass originates from spontaneous symmetry breaking, it is most natural to consider a particle with a technically natural mass such as a fermion. We therefore use as a specific example a toy model of thermal leptogenesis, in which a lepton asymmetry is first generated via the decays of singlet right-handed neutrinos (RHNs) and is then transmitted to baryons via $B + L$ -violating sphaleron processes [19]. However, we emphasize that the results we derive apply more generally to any model with a phase transition with asymmetry generation from out-of-equilibrium decay, and we therefore focus on a simpler toy version of the theory comprising only two generations of each type

of fermion. We also allow the Yukawa couplings to deviate from the naïve see-saw values to obtain results applicable to more general models, and we ignore subtleties such as spectator processes and $\mathcal{O}(1)$ factors associated with transmitting the lepton asymmetry to baryons. Our findings can be trivially extended to apply to other theories, including specific models of neutrino masses.

The new field content is a pair of right-handed neutrinos, N_I , each of which can decay into the left-handed lepton doublets, L_α , and the Higgs field, H . There are many excellent reviews of this subject that provide more details than provided here; see, for example, Ref. [40]. The Lagrangian is

$$\mathcal{L} = F_{\alpha I} \bar{L}_\alpha H^* N_I + \frac{M_I}{2} \bar{N}_I^c N_I + \text{h.c.} + \mathcal{L}_{\text{kinetic}}. \quad (1)$$

The Yukawa couplings above are specified in the basis where the N_I mass is diagonal. The complex Yukawa matrix has a physical phase if there are at least two generations of N and L , giving rise to CP violation. An asymmetry in L_α is generated when $N_I \rightarrow L_\alpha H$ occurs at a faster rate than $N_I \rightarrow \bar{L}_\alpha H^*$. The difference in rates arises due to interference of tree and loop contributions to decay, and the lepton asymmetry in flavour α produced per N_I decay is characterized by [41]

$$\begin{aligned} \varepsilon_I^\alpha &\equiv \frac{\Gamma(N_I \rightarrow L_\alpha H) - \Gamma(N_I \rightarrow \bar{L}_\alpha H^*)}{\sum_\beta [\Gamma(N_I \rightarrow L_\beta H) + \Gamma(N_I \rightarrow \bar{L}_\beta H^*)]} \\ &= \frac{1}{8\pi} \frac{1}{(F^\dagger F)_{II}} \sum_{J \neq I} \left[\text{Im} \left[(F^\dagger F)_{IJ} F_{I\alpha}^\dagger F_{\alpha J} \right] g(x_{IJ}) + \text{Im} \left[(F^\dagger F)_{JI} F_{I\alpha}^\dagger F_{\alpha J} \right] \frac{1}{1 - x_{IJ}} \right], \end{aligned} \quad (2)$$

where

$$x_{IJ} = \frac{M_J^2}{M_I^2}, \quad g(x) = \sqrt{x} \left[\frac{1}{1-x} + 1 - (1+x) \log \left(\frac{1+x}{x} \right) \right]. \quad (3)$$

ε_I^α is enhanced in the limit $M_I \rightarrow M_J$ due to a resonance in the self-energy contribution to the asymmetry. The above expression is valid in the limit $|M_I^2 - M_J^2| \gg \max(M_I \Gamma_I, M_J \Gamma_J)$, while in the fully degenerate limit it is important to include effects of oscillations among mass eigenstates (see Appendix A for generalizations of Eq. (2) in this limit) [42, 43].

The asymmetry in L_α is produced via the decays of $N_I \rightarrow L_\alpha H$, while it is destroyed by the washout processes of inverse decay ($H L_\alpha \rightarrow N_I$) and off-shell $2 \leftrightarrow 2$ scattering (such as $H L_\alpha \leftrightarrow H^* \bar{L}_\beta$). In the semi-classical limit, the evolution of particle abundances can be modelled by Boltzmann equations. These are most simply expressed in terms of the number density normalized to the entropy density, $Y_i \equiv n_i/s$. Assuming that the interactions with L_α , H provide the only decay mode for N_I , then the Boltzmann equations for the evolution of Y_N and the lepton asymmetry in flavour α , $Y_{\Delta L_\alpha} \equiv Y_{L_\alpha} - Y_{\bar{L}_\alpha}$ are

$$\begin{aligned} \frac{dY_{N_I}}{dt} &= -\langle \Gamma_{N_I} \rangle (Y_{N_I} - Y_{N_I}^{\text{eq}}), \\ \frac{dY_{\Delta L_\alpha}}{dt} &= \sum_I \varepsilon_I^\alpha \langle \Gamma_{N_I} \rangle \text{Br}(N_I \rightarrow \alpha) (Y_{N_I} - Y_{N_I}^{\text{eq}}) - \sum_I \langle \Gamma_{N_I} \rangle \text{Br}(N_I \rightarrow \alpha) \frac{Y_{N_I}^{\text{eq}}}{2Y_L^{\text{eq}}} Y_{\Delta L_\alpha}, \end{aligned} \quad (4)$$

where $\langle \Gamma_{N_I} \rangle$ is the thermally averaged total N_I width and $\text{Br}(N_I \rightarrow \alpha)$ is the branching fraction of $N_I \rightarrow L_\alpha H + \bar{L}_\alpha H^*$. Note that the asymmetry is defined as the sum over the asymmetries in each doublet component. Detailed definitions of the various terms in the Boltzmann equation are provided in Appendix B.

We can re-write the second Boltzmann equation as

$$\frac{dY_{\Delta L_\alpha}}{dt} = - \sum_I \varepsilon_I^\alpha \text{Br}(N_I \rightarrow \alpha) \frac{dY_{N_I}}{dt} - \sum_I \langle \Gamma_{N_I} \rangle \text{Br}(N_I \rightarrow \alpha) \frac{Y_{N_I}^{\text{eq}}}{2Y_L^{\text{eq}}} Y_{\Delta L_\alpha}, \quad (5)$$

which makes clear that an asymmetry of ε_I^α is produced for every decay of N_I (weighted by the branching fraction of N_I into flavour α). The second term destroys the asymmetry via inverse decays; because the L_α

and H must draw sufficient energy from the bath to re-constitute N_I , the rate is Boltzmann-suppressed for $M_I \gg T^1$.

The solution to the Boltzmann equation for the asymmetry in flavour α , Eq. (5), at very late times is

$$Y_{\Delta L_\alpha}^\infty = - \sum_I \varepsilon_I^\alpha \text{Br}(N_I \rightarrow \alpha) \int_0^\infty dt' \frac{dY_{N_I}}{dt'} \exp \left[- \int_{t'}^\infty dt'' \Gamma_W^\alpha(t'') \right], \quad (6)$$

where $\Gamma_W^\alpha(t)$ is the rate of washout processes that destroy the asymmetry in L_α ,

$$\Gamma_W^\alpha(t) = \sum_I \Gamma_{W,I}^\alpha \equiv \sum_I \frac{Y_{N_I}^{\text{eq}}}{2Y_{L_\alpha}^{\text{eq}}} \langle \Gamma_{N_I} \rangle \text{Br}(N_I \rightarrow \alpha). \quad (7)$$

The solution Eq. (6) can be understood as follows: in the time interval $[t', t' + \Delta t']$, an asymmetry in L_α is generated that is equal to the net number of decays of N_I in this interval multiplied by ε_I^α . This asymmetry, however, is exponentially damped by inverse decays occurring at times $t > t' + \Delta t'$. Once the integral of the washout rate falls below 1 (approximately when $\Gamma_W^\alpha(t')$ falls below the Hubble rate $H(t')$), the asymmetry destruction processes cease to be effective and any asymmetry generated after this time is preserved.

The dependence of the solution on the model parameters depends on whether washout processes were ever important or not. These are classified as the strong and weak washout regimes, respectively:

Weak Washout: In this scenario, the integrated washout in the exponent of Eq. (6) is always negligible during the epoch of net N_I decays (*i.e.*, $M_I > T$); this is because the Hubble expansion of the universe is always faster than inverse decays, $H(t) > \Gamma_W(t)$, during this period. In this case,

$$Y_{\Delta L_\alpha}^\infty \approx - \sum_I \varepsilon_I^\alpha \text{Br}(N_I \rightarrow \alpha) \int_0^\infty dt' \frac{dY_{N_I}}{dt'} = \sum_I \varepsilon_I^\alpha \text{Br}(N_I \rightarrow \alpha) Y_{N_I}(0) \quad (8)$$

Thus, every net N_I decay into L_α efficiently contributes to the lepton asymmetry by a factor of ε_I^α . Note, however, that the result is sensitive to the abundance of N_I at early times, $Y_{N_I}(0)$: because the couplings to L_α are insufficient to bring the N_I into equilibrium at early times, its initial abundance and hence the lepton asymmetry depend strongly on whatever other scattering processes could produce N_I at temperatures $T > M_I$.

Strong Washout: In this scenario, there is a period of time in which the lepton-number-violating scattering processes are rapid compared to the expansion rate of the universe. This is a typical scenario due to the fact that the expansion rate is suppressed by the Planck scale and typically very small compared to reaction rates unless lepton-number-violating couplings are very small. Because of frequent decays and inverse decays, thermal equilibrium is established for the N_I abundances ($Y_{N_I} \approx Y_{N_I}^{\text{eq}}$) in the strong washout scenario. As T cools below M_I , the asymmetry produced during the early decays of N_I are rapidly damped away by washout processes. The importance of washout for flavour α is typically characterized by the following quantity:

$$\mathcal{K}_I^\alpha \equiv \frac{\Gamma_{N_I} \text{Br}(N_I \rightarrow \alpha)}{H(T = M_I)}, \quad (9)$$

where \mathcal{K}_I^α is larger for stronger washout.

As the universe cools below M_I , the rate of inverse decays (and hence the washout rate) is Boltzmann suppressed $Y_{N_I}^{\text{eq}} \sim e^{-M_I/T}$. Due to the rapidly falling exponential, the total washout rate eventually slows to equal the rate of expansion at a temperature T_* , defined implicitly by $\Gamma_W^\alpha(T_*) = H(T_*)$. From this point onward, any asymmetry in L_α produced from N_I decays is preserved, and we can estimate the final asymmetry produced from N_I decays as

$$Y_{\Delta L_\alpha}^\infty \sim \sum_I \varepsilon_I^\alpha \text{Br}(N_I \rightarrow \alpha) Y_{N_I}^{\text{eq}}(T_*). \quad (10)$$

¹We neglect here higher-order washout terms $\sim |F|^4$ because, for the relatively small couplings we consider, these rates provide only a very minor correction to the $\mathcal{O}(|F|^2)$ terms, and we have verified this in our numerical solutions.

In the case of a sufficiently hierarchical spectrum of N_I particles, with $M_1 \ll M_{J \neq 1}$, the total washout rate decouples when only the lightest N_1 has an appreciable abundance due to the stronger Boltzmann suppression for the processes involving $N_{J \neq 1}$. In this case, the washout is also dominated by the rate $\Gamma_{W,1}$, which in turn depends on the width Γ_{N_1} . Then, using the definition of T_* and the asymmetry from Eq. (10), we may estimate the total asymmetry as

$$Y_{\Delta L_\alpha}^\infty \sim \varepsilon_1^\alpha \text{Br}(N_1 \rightarrow \alpha) Y_{N_1}^{\text{eq}}(T^*) \sim \frac{2\varepsilon_1^\alpha \text{Br}(N_1 \rightarrow \alpha) Y_{L_\alpha}^{\text{eq}}}{(z_1^*)^2 \mathcal{K}_1^\alpha}. \quad (11)$$

where we have defined $z_1^* \equiv M_1/T_*$. Due to the exponential damping of the washout rate from inverse decays, z_1^* typically lies between 1 – 10. Recall that $Y_{L_\alpha}^{\text{eq}}$ is the abundance of the lepton, which is massless for temperatures above the weak scale and is approximately constant during leptogenesis.

The key property to note is that the final asymmetry in L_α is inversely proportional to the washout strength \mathcal{K}_1^α . A larger washout strength \mathcal{K}_1^α implies that washout remains effective down to a lower temperature, reducing the number of N_1 decays that can generate an asymmetry². In Eq. (11), z_1^* can be determined by iteratively solving the above equation in the same manner as for the calculation of dark matter chemical decoupling in thermal freeze-out models [44].

We derived the scaling relation Eq. (11) under the assumption that the only contribution to the final L_α asymmetry comes from decays after washout freeze-out. This neglects earlier decays that are partially washed out, and these can contribute an $\mathcal{O}(1)$ fraction of the total. A better estimate is obtained by evaluating Eq. (6) in the steepest-descent approximation, which gives a similar parametric dependence but without requiring the iterative solution for z_1^* [45]:

$$Y_{\Delta L_\alpha}^\infty \approx \varepsilon_1^\alpha \text{Br}(N_1 \rightarrow \alpha) Y_{L_\alpha}^{\text{eq}} \left(\frac{1}{2\mathcal{K}_1^\alpha} \right)^{1.16}. \quad (12)$$

Our discussion so far has focused on the asymmetry in a particular flavour, L_α . Of course, we are actually interested in the *total* lepton number obtained by summing over lepton flavours. For a generic theory without any hierarchical couplings, one might expect ε_1^α and \mathcal{K}_1^α are approximately flavour independent, in which case one would get a total lepton asymmetry on the order of the individual flavour asymmetries and the same scaling dependence. In specific cases, hierarchies in flavour couplings can give rise to non-trivial effects on the asymmetry, in which case our naïve scaling arguments break down [26]. However, the scaling derived above holds for many models and provides a useful analytic approximation for understanding the physical effects of a time-varying mass.

We may obtain an explicit analytic expression for the washout factor in terms of the parameters of the theory by substituting the temperature dependence of the Hubble rate in a radiation-dominated universe with g_* relativistic degrees of freedom,

$$H \approx 1.66 \sqrt{g_*} \frac{T^2}{m_{\text{P}}}, \quad (13)$$

where $m_{\text{P}} = 1.22 \times 10^{19}$ GeV is the Planck mass. Using the zero-temperature decay rate of the N_I in the limit of massless products,

$$\Gamma_{N_I} = \frac{(F^\dagger F)_{II} M_I}{8\pi}, \quad (14)$$

this gives for the washout factor,

$$\mathcal{K}_I^\alpha \approx \frac{|F_{\alpha 1}|^2 m_{\text{P}}}{13.28 \pi \sqrt{g_*} M_I}. \quad (15)$$

²Also, z_1^* is larger for stronger washout; however, this dependence is logarithmic and this is not the dominant effect on the asymmetry in the strong washout limit.

To conclude this section, we discuss which of the above parameter regimes is most likely to be affected when M_I changes due to a phase transition. The weak washout scenario already features a strong departure from thermal equilibrium, and so an additional departure from equilibrium due to a changing mass is unlikely to increase the asymmetry. Indeed, the dominant effect of a phase transition on the weak washout regime is the existence of new couplings between N_I and the symmetry breaking sector that can modify its abundance prior to the epoch of leptogenesis. By contrast, the strong washout regime features lepton-number-violating processes that are in equilibrium and inhibit the generation of an asymmetry for temperatures $T > T_*$. A phase transition may provide an additional departure from thermal equilibrium, modifying the dynamics of asymmetry generation. Therefore, in what follows we focus predominantly on the strong washout regime, but comment where relevant on the effects of the new interactions on the weak washout limit.

3 Asymmetry Generation with a Phase Transition

3.1 Time-Dependent Majorana Mass

When an asymmetry is generated via the decay of a heavy particle, a departure from equilibrium occurs in two, interconnected ways. The cooling of the universe below M_I results in the net decay of N_I into the lighter lepton species, allowing for the generation of an asymmetry. At the same time, the cooling also suppresses inverse decays that wash out the asymmetry, allowing the accumulation of a substantial asymmetry.

If the Majorana mass, M_I , originates from a phase transition in the early universe, this can provide an additional departure from equilibrium if the mass changes on time scales that are fast relative to the Hubble expansion rate. The rapid increase of M_I at the phase transition tends to suppress washout processes more quickly than the Hubble expansion alone, meaning that an asymmetry generated by the decays of N_I may not have time to relax to zero as fully as in the conventional strong washout scenario that is our main focus.

For the remainder of the paper, we replace the Majorana mass for N_I with a coupling to a symmetry-breaking scalar Φ :

$$\mathcal{L}_{\text{mass}} = \frac{y_I}{2} \Phi \bar{N}_I^c N_I + \text{h.c.} + \mathcal{L}_\Phi. \quad (16)$$

If N_I possesses an appropriate discrete or continuous symmetry, a tree-level mass term as in Eq. (1) is forbidden and the coupling to Φ provides the only contribution to the N_I mass after symmetry breaking. The Majorana masses of the right-handed neutrinos are now

$$M_I(t) = y_I \langle \Phi(t) \rangle. \quad (17)$$

In this section, we are agnostic about the details of the symmetry-breaking field Φ and its dynamics. In particular, we assume that Φ is simply a time-dependent background field and that all new states associated with this symmetry breaking are decoupled at the time of baryogenesis. While this is not a realistic assumption [28, 29], it does allow us to isolate the effects of the background-field phase transition from other dynamics of the new scalar interactions. With this assumption hypothesis, the generation of the baryon asymmetry is modelled by the same Boltzmann equations in Eq. (4), but with time-dependent values for masses of the N_I . We return to the effects of N_I scattering into Φ in Sec. 4.

Our study of the effects of the phase transition on baryogenesis requires some ansatz for the form of the phase transition. For now, we restrict ourselves here to simplistic ansätze for Φ as a function of temperature (and hence time) that make clear the influence of the phase transition, and defer a discussion of particular models (from which the evolution of Φ during the phase transition is calculable) to Sec. 5. While realistic phase transitions have more complicated mass profiles, our ansätze allow for an intuitive understanding of how the asymmetry depends on the nature of the phase transition. We consider different scenarios: a very fast first-order phase transition, a second-order phase transition, and a slowly evolving scalar which remains constant over the time scales of leptogenesis but differs in value between the time of leptogenesis and the

present. The slow evolution, although not providing an enhanced departure from thermal equilibrium, can be an interesting case study for thermal leptogenesis because it modifies the relation between SM neutrino masses and M_I in the early universe vs. their values today. This has been argued to allow for enhanced asymmetries [46, 32], and we include a study of this scenario for completeness.

For the phase transitions, the time-dependent background field profiles we study in this section are:

$$\text{First order : } \Phi(T) = \Phi_0 \theta(T_c - T), \quad (18)$$

$$\text{Second order : } \Phi(T) = \Phi_0 \sqrt{1 - \frac{T^2}{T_c^2}} \theta(T_c - T), \quad (19)$$

where T_c is the critical temperature of the phase transition and a free parameter of the model. These background-field profiles lead to time-dependent masses that are substituted into the Boltzmann equations. The time-varying masses appear in the Boltzmann equations in a few places: in the expressions for the equilibrium N_I abundance, in the thermally averaged widths, and in the CP -violating source terms driving the creation of the asymmetry (ε_I^α). According to Eq. (2), however, ε_I^α is sensitive only to the ratios among masses. Since $x_{IJ} = y_J^2/y_I^2$ is independent of time, this suggests that the CP -violating sources are time independent as well. This is true only under the approximations that render Eq. (2) valid, namely that the time-dependence of the CP source due to coherence effects is much shorter than due to other scattering processes [47, 48]. We restrict ourselves to model parameters for which this is true.

3.2 First-Order Phase Transition

Prior to the start of the phase transition, all fields are massless at tree level. However, N_I acquires a non-trivial dispersion relation from propagating through the hot, dense plasma. The N_I remain relativistic as the universe cools and their number density does not depart from thermal equilibrium. Thus, no asymmetry is generated in the unbroken phase.

In the limit of a very fast phase transition, the masses of all fields suddenly turn on at $T = T_c$. In this phase, the mass is

$$M_I^2(T < T_c) = y_I^2 \Phi_0^2, \quad (20)$$

where Φ_0 is the zero-temperature vacuum expectation value. We neglect thermal effects on the N_I propagation: this is reasonable since the net N_I number density does not change until $M_I(T) = T$ and hence no leptogenesis occurs until later than this time. For a perturbative theory, the thermal corrections to the N_I mass in the high-temperature expansion are therefore subdominant to the tree-level term for $T < M_I(T)$. We define the zero-temperature mass as $M_I^0 \equiv y_I \Phi_0$.

For $T_c \gg M_I^0$, the effect of the phase transition on the mass or number density of N_I is negligible. In other words, the N_I retain an unchanging equilibrium abundance throughout the phase transition. The largest contribution to the asymmetry from N_I decay does not occur until washout goes out of equilibrium at a scale $T_* \lesssim M_I^0 \ll T_c$, and therefore the phase transition has no effect on leptogenesis.

Conversely, for $T_c \ll T_* \lesssim M_I^0$, the washout suddenly turns off when the mass changes. Since we are considering N_I in the strong washout regime ($\mathcal{K}_I^\alpha = \Gamma_{N_I} \text{Br}(N_I \rightarrow \alpha)/H(M_I) > 1$ for some α), the N_I rapidly decay to their new equilibrium abundance, giving rise to a net asymmetry:

$$Y_{\Delta L_\alpha} = \sum_I \varepsilon_I^\alpha \text{Br}(N_I \rightarrow \alpha) Y_{N_I}(T_c). \quad (21)$$

In contrast, the washout processes suffer a Boltzmann suppression, $\Gamma_W^\alpha \sim \Gamma_{N_I} \text{Br}(N_I \rightarrow \alpha) e^{-M_I^0/T_c}$, and for $T_c \ll T_* < M_I^0$ the washout processes are ineffective. In this case, Eq. (21) gives the exact result for the final asymmetry. Using the simple analytic solution to the asymmetry for leptogenesis in the absence of a phase transition, Eq. (11), we find that the ratio of asymmetries is:

$$\frac{Y_{\Delta L_\alpha}^{\text{P.T.}}}{Y_{\Delta L_\alpha}^{\text{no P.T.}}} \approx \frac{\sum_I \varepsilon_I^\alpha Y_{N_I}(T_c)}{Y_{L_\alpha}^{\text{eq}} \sum_I 2\varepsilon_I^\alpha [\mathcal{K}_I^\alpha (M_I^0)^2/T_*^2]^{-1}} \quad (T_* > T_c), \quad (22)$$

In particular, we see that the ratio of asymmetries scales like \mathcal{K}_I^α : the larger the couplings leading to N_I decay, the more pronounced the effect of a phase transition is on the asymmetry by suppressing washout. Eq. (22) is only valid in the limit $T_c \ll T_* < M_I^0$ such that all washout is negligible; it is possible to analytically solve for the asymmetry ratio in the intermediate case $T_c \sim T_*$. If $T_c \gg T_*$, the N_I equilibrate in the new phase and the asymmetry reverts to the result in the absence of a phase transition.

In order to evaluate Eq. (22), we must know the abundance of N_I immediately after the phase transition, $Y_{N_I}(T_c)$. In the ideal case where the mass of N_I changes instantaneously and homogeneously throughout space as described in Eq. (18), the abundance of N_I does not have the opportunity to react to the change, and so $Y_{N_I}(T_c) = Y_{L_\alpha}$ (*i.e.*, the abundance is the same as for a massless species). We then find an enhancement in the asymmetry $\propto \mathcal{K}_I^\alpha$ for the case of a first-order phase transition relative to a time-independent mass.

For realistic models, however, we know that first-order phase transitions proceed through bubble nucleation, followed by the rapid expansion of the bubble walls. The result is a mass profile possessing a spatial gradient in addition to the time dependence. Assuming the bubble nucleates at the origin, and in the thin-walled approximation, the N_I mass profile at position \vec{r} has the form

$$M_I(T, \vec{r}) \approx M_I^0 \theta(T_c - T) \theta[v_w(t - t_c) - |\vec{r}|], \quad (23)$$

where v_w is the bubble-wall velocity and t_c is the time of the phase transition. As the bubble wall expands, particles in the unbroken phase must either propagate through the wall, or be reflected at the phase boundary. If $T_c \gtrsim M_I^0$, then the N_I in the plasma have sufficient energy to penetrate the bubble wall, and an $\mathcal{O}(1)$ fraction propagate into the broken phase. In this limit, however, there is no appreciable effect of the phase transition on the asymmetry since the N_I retain a near-equilibrium abundance during the phase transition, and the bulk of the asymmetry is not generated until after washout interactions cease at a time well after the phase transition.

Conversely, if $T_c \ll M_I$, then the vast majority of N_I particles cannot penetrate the bubble wall and are reflected; conservation of energy dictates that only those with typical momentum $k \sim M_I^0$ can enter the bubble [49], and the abundance of these modes is highly Boltzmann suppressed by $e^{-M_I^0/T_c}$. The yield of N_I immediately after the passage of the bubble walls is

$$Y_{N_I}(M_I = M_I^0, T_c) \approx Y_{N_I}(M_I = 0, k > M_I^0) \approx \frac{1}{2} \left(\frac{M_I^0}{T_c} \right)^2 e^{-M_I^0/T_c} Y_{N_I}(M_I = 0). \quad (24)$$

We find that the asymmetry is exponentially suppressed due to the same Boltzmann suppression of N_I modes propagating through the bubble wall. Using the definition of T_* as the temperature at which $\Gamma_W^\alpha(T_*) = H(T_*)$, and considering N_1 as the dominant contributor to both the asymmetry and washout to obtain the approximate scaling behaviour, we can express the baryon asymmetry ratio as

$$\frac{Y_{\Delta L_\alpha}^{\text{P.T.}}}{Y_{\Delta L_\alpha}^{\text{no P.T.}}} \sim \frac{\mathcal{K}_1^\alpha}{4} \left(\frac{M_1^0}{T_*} \right)^2 \left(\frac{M_1^0}{T_c} \right)^2 e^{-M_1^0/T_c} \quad (T_* > T_c). \quad (25)$$

According to our analytic estimate, we see that if the phase transition occurs at $T_c \ll T_*$, there is an exponential suppression of the asymmetry relative to the scenario with no phase transition. By contrast, if $T_c \gtrsim T_*$, then this formula is no longer valid and instead the N_I equilibrate prior to the generation of the asymmetry and there is no effect of the phase transition. In the intermediate case, $T_c \sim T_*$, it may be possible to realize a small enhancement of the asymmetry due to the phase transition, but this is $\mathcal{O}(1)$ because M_I/T_* depends only logarithmically on the decay rate. Thus, it appears that a first-order phase transition either has no effect if it happens prior to N_I going out of equilibrium, or it leads to an exponential suppression of the asymmetry if it occurs after the N_I depart from equilibrium.

We derived the change in the asymmetry from the phase transition in Eq. (25) with several simplifying assumptions, such as looking at the contribution of only one flavour of L_α and N_I . The result, however, approximately holds even when solving the full Boltzmann equations numerically. We consider a system of two flavours of N_I and L_α , generate a random complex Yukawa matrix with characteristic real and imaginary parts of order 10^{-2} (shown in Eq. (100)), and solve the resulting Boltzmann equations assuming initial conditions

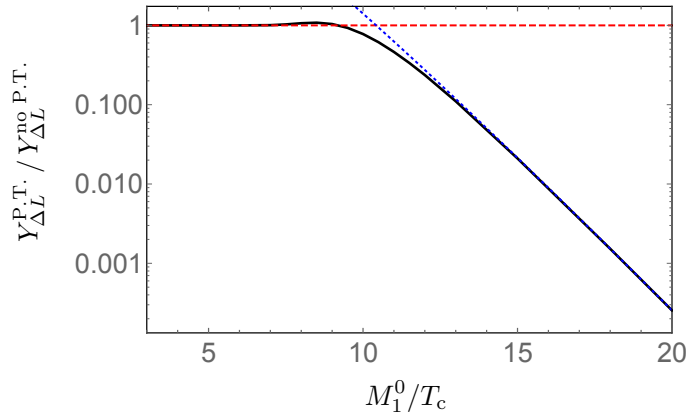


Figure 1: Ratio of total lepton number asymmetry, $Y_{\Delta L}$, with a **first-order phase transition** relative to the constant-mass case. Only N_I modes that are sufficiently energetic to propagate through the bubble wall are considered for generating the asymmetry. The solid curve indicates the numerical solution of the Boltzmann equation, while the dotted blue line is a fit to Eq. (25), and the dashed red line illustrates the ratio of unity expected when T_c is high enough that the N_I equilibrate after the phase transition. For the specific numerical results plotted here, we take $M_1 = M_2/2 = 10^9$ GeV, and the Yukawa matrices are generated as random matrices with typical real and imaginary parts of 10^{-2} , Eq. (100).

at T_c of $Y_{N_I}(T_c) = Y_{N_I}(M = 0, T_c, k > M_I^0)$ for the massive fermions in the broken phase. We compute the total lepton number asymmetry in both the case where the mass turns on suddenly and the constant-mass scenario, and their ratio is shown in Fig. 1. We see that, at large M_I^0/T_c , the exponential suppression of the asymmetry predicted by Eq. (25) is evident, while at large M_I^0/T_c , the N_I equilibrate in the broken phase and the asymmetry is essentially unchanged.

In our discussion, we have focused exclusively on the effects of the changing mass, $M_I(T)$, on the baryon asymmetry from a first-order phase transition. There may be other effects of the bubble-wall dynamics that can lead to successful baryogenesis apart from decays [31, 34, 50, 37, 35, 36].

3.3 Second-Order Phase Transition

We now consider phase transitions where Φ relaxes homogeneously to its zero-temperature vacuum with no discontinuity in the order parameter. Such phase transitions give rise to a temperature-dependent mass with a profile like

$$M_I(T) = M_I^0 \left(1 - \frac{T^2}{T_c^2}\right)^n \theta(T_c - T). \quad (26)$$

The mass vanishes until a temperature T_c , at which point the mass smoothly transitions to the zero-temperature value M_I^0 . The power of n depends on the details of the phase transitions: for example, a second-order phase transition that occurs due to the competition between thermal corrections to a scalar mass and the tree-level term derived in the high-temperature expansion has $n = 1/2$ (as with the SM Higgs). Higher-order corrections and deviations from the high- T expansion modify the above form, but we use this simple ansatz to illustrate the parametric behaviour of the baryon asymmetry.

Conventionally, second-order phase transitions are believed to not provide a strong departure from thermal equilibrium beyond Hubble expansion. The reason is that the change in mass occurs continuously due to a change in T , which itself arises from Hubble expansion. Therefore, the change in mass is expected to be comparable to the characteristic expansion time scale. A simple example shows that this is not always true,

however. If we compute the time derivative of our mass ansatz for $T < T_c$, we find

$$\frac{dM_I}{dt} = 2Hn M_I(T) \frac{T^2}{T_c^2 - T^2}. \quad (27)$$

For $T_c > T \geq T_c/\sqrt{2n+1}$, the mass is changing faster than the Hubble expansion, meaning that processes sensitive to M_I could deviate from equilibrium more sharply within this window of temperatures. In other words, for $T \sim T_c$ the mass changes faster than processes with typical timescale $\Gamma \sim H$ can respond to the change.

Washout processes go out of equilibrium when their rate becomes slower than their own rate of change,

$$\frac{1}{\Gamma_W^\alpha} \frac{d\Gamma_W^\alpha}{dt} \approx -\Gamma_W^\alpha. \quad (28)$$

Once this is satisfied, the washout processes turn off faster than they can appreciably destroy the baryon asymmetry. We now derive an estimate for when this condition is satisfied taking Maxwell-Boltzmann statistics for simplicity in the approximate analytic results. Using Eq. (7) and the results of Appendix B, we can write

$$\Gamma_W^\alpha \approx \frac{1}{32\pi T^2} \sum_I |F_{\alpha I}|^2 M_I^3 K_1(M_I/T), \quad (29)$$

where K_1 is the modified Bessel function of the first kind. According to our earlier arguments, the phase transition only has a major effect in the strong washout limit. In this case, we expect washout to decouple for $M_I/T \gg 1$. Taking this limit, we find a compact form for the derivative of the washout rate:

$$\frac{d\Gamma_W^\alpha}{dt} = -H \sum_I \Gamma_{W,I}^\alpha \frac{M_I}{T} \left(1 - \frac{T}{M_I} \frac{dM_I}{dT}\right). \quad (30)$$

We evaluate this in the hierarchical case where a single species, N_J , dominates the washout for simplicity. We first evaluate the condition for the mass-independent scenario, and then proceed to the mass-varying case.

Time-Independent Mass: In the case of constant mass and one species, J , dominating the washout, we find that Eq. (28) reduces to the usual requirement that washout decouples when the washout rate falls below the Hubble expansion rate,

$$\Gamma_W^\alpha(T_*) \approx H(T_*) \frac{M_J^0}{T_*}, \quad (31)$$

where T_* is the temperature at which this equality holds. This condition can be formulated entirely in terms of the washout factor, $\mathcal{K}_J^\alpha = \Gamma_{N_J}^\alpha/H(M_J^0)$, and the dimensionless ratio $z_J^* \equiv M_J^0/T_*$,

$$\frac{\mathcal{K}_J^\alpha}{4} z_J^{*3} K_1(z_J^*) = 1. \quad (32)$$

There is no explicit mass dependence, and this explains why the asymmetry in each flavour can be estimated simply in terms of \mathcal{K}_J^α in Eq. (11).

Time-Dependent Mass: If, instead, the mass derivative term dominates the expression for the change in washout (*i.e.*, $dM_J/dT > M_J/T$), we find the condition of washout freeze-out in the single-flavour limit changes to

$$\Gamma_W^\alpha(T'_*) = -H(T'_*) \frac{dM_J(T'_*)}{dT}, \quad (33)$$

where T'_* is defined as the temperature at which this equality holds. We see that a large derivative for the time-dependent mass results in washout decoupling at an earlier time than might otherwise be expected. Expressing

this equality purely in terms of the washout factor \mathcal{K}_J^α and the dimensionless ratio $z'_J \equiv M_J(T'_*)/T'_*$, we can write the condition of washout freeze-out as

$$-\frac{\mathcal{K}_J^\alpha}{4} \frac{M_J^0}{T'_*} \left(\frac{dM(T'_*)}{dT} \right)^{-1} z_J'^3 K_1(z'_J) = 1. \quad (34)$$

We therefore find that the washout condition in the mass-varying scenario is the same as for a time-independent mass, provided we substitute the factor \mathcal{K}_J^α for an **effective washout factor**:

$$(\mathcal{K}_J^\alpha)^{\text{eff}} \equiv -\mathcal{K}_J^\alpha \frac{M_J^0}{T'_*} \left(\frac{dM_J(T'_*)}{dT} \right)^{-1}. \quad (35)$$

Because everything else in the condition for washout freeze-out depends only on the dimensionless ratio $M_J(T)/T$, the asymmetry scales like

$$Y_{\Delta L} \sim \frac{1}{(\mathcal{K}_J^\alpha)^{\text{eff}}}. \quad (36)$$

Consequently, if the mass changes very rapidly, $(\mathcal{K}_J^\alpha)^{\text{eff}} \ll \mathcal{K}_J^\alpha$, this results in an enhancement of the asymmetry over the time-independent scenario.

To obtain an estimate of $(\mathcal{K}_J^\alpha)^{\text{eff}}$ (and hence an analytic scaling for the lepton asymmetry), we must determine the temperature T'_* relative to known scales in the theory. The second-order phase transition only has an effect if $M_J(T)$ varies rapidly with T , and from Eq. (27) we see that this occurs only for $T \approx T_c$. For a typical second-order phase transition, the T -dependence of the mass in the high- T expansion is given in Eq. (26) with $n = 1/2$ (see also Eq. (19)). In this case, we find

$$\frac{dM_J}{dT} \approx -\frac{(M_J^0)^2}{z_J T_c^2} \quad (37)$$

where we recall that $z_J = M_J(T)/T$. Although dM/dT nominally diverges at $T = T_c$, no asymmetry is generated at this time because net decays do not start occurring until $M_J(T) \approx T$. Because washout decouples exponentially quickly for $T < M(T)$, we expect that $z_{J*} \sim 1 - 10$. We therefore find that the transition is fastest (and the asymmetry is maximized) for $M_J^0 \gg T_c$.

T'_* becomes closer to T_c for faster transitions, and the enhancement of the asymmetry grows due to the suppression of the effective washout Eq. (35). The effective washout factor is then

$$(\mathcal{K}_J^\alpha)^{\text{eff}} \approx \mathcal{K}_J^\alpha z_{J*} \frac{T_c}{M_J^0}. \quad (38)$$

Asymmetry Ratio: Since $Y_{\Delta L}^\alpha \sim 1/(\mathcal{K}_J^\alpha)^{\text{eff}}$, we find a *linear enhancement* of the asymmetry for a delayed transition $M_J \gg T_c$ in the single-flavour limit:

$$\frac{Y_{\Delta L_\alpha}^{\text{P.T.}}}{Y_{\Delta L_\alpha}^{\text{no P.T.}}} \sim \frac{M_J^0}{T_c} z_J^*. \quad (39)$$

The enhancement grows linearly until the phase transition occurs so rapidly that washout reactions have no time to respond to the changing mass. At this point, we enter an “effective” weak washout limit, and as shown in Eq. (8), the asymmetry is determined exclusively by the CP -violating sources and the relativistic abundance of the massless N_J prior to the phase transition³:

$$(Y_{\Delta L}^\alpha)^{\text{max}} = \varepsilon_J^\alpha \text{Br}(N_J \rightarrow \alpha) Y_{N_J}^{\text{eq}}(T > T_c) \approx \frac{45}{g_* \pi^4} \varepsilon_J^\alpha \text{Br}(N_J \rightarrow \alpha). \quad (40)$$

For even faster phase transitions, the asymmetry no longer has any dependence on the critical temperature and approaches a constant.

³We have assumed that the number of entropic degrees of freedom is the same as the number of radiation degrees of freedom.

$$y_1 = 1, M_1 = M_2/2 = 10^9 \text{ GeV}$$

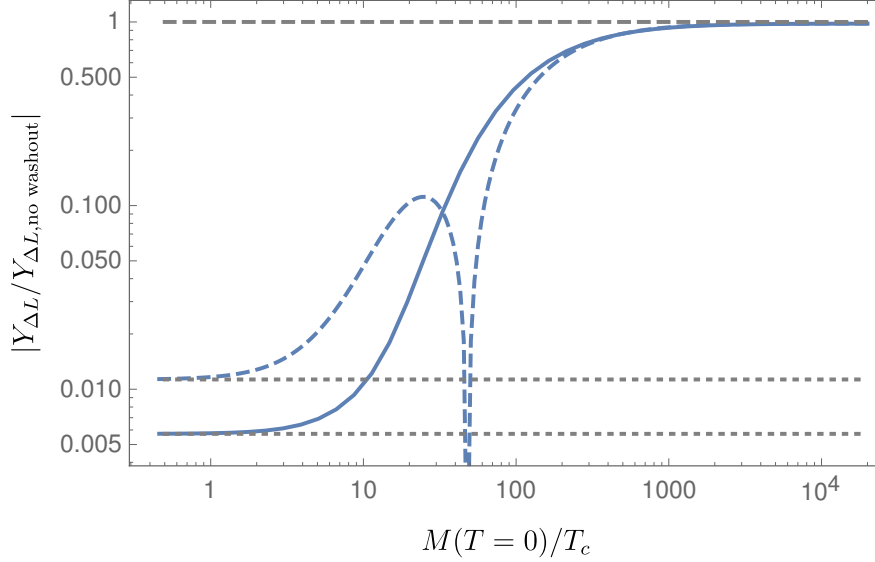


Figure 2: Dependence of the asymmetry on the critical temperature of a **second-order phase transition** giving rise to RHN masses, Eq. (41). Results are shown in the tree-level approximation with leading temperature corrections. The dashed-gray and dotted-gray lines show the asymptotic results expected for zero washout and constant masses, respectively. We set $y_1 = 1$, $M_1 = M_2/2 = 10^9$ GeV, and calculate the asymmetry for two random choices of Yukawa matrix F (given by Eq. (101) and (102) in Appendix E) with typical real and imaginary parts of the order of 10^{-3} . For the solid blue line, the sign of the asymmetry for constant M_I does not change in the limit of zero washout, as opposed to the case of the dashed blue line, for which flavour effects change the sign of the asymmetry.

Numerical Study: The above analytic estimates were obtained in the single-flavour limit to obtain approximate scaling relations. However, we now examine numerically a 3×2 flavour system as would be expected for a model of RHNs generating the observed neutrino masses and mixings. We consider a model with right-handed neutrinos, N_J , and a symmetry-breaking scalar Majoron Φ with the following interactions:

$$\mathcal{L}_{\text{mass}} \supset -\frac{y_I}{2} \Phi \bar{N}_I^c N_I + \text{h.c.} + m_\Phi^2 \Phi^\dagger \Phi - \frac{\lambda}{4} (\Phi^\dagger \Phi)^2, \quad (41)$$

with additional operators forbidden by means of appropriate continuous or discrete symmetries. The mass profiles for the RHNs, $M_I(T)$, can be determined from the leading order contributions to the high-temperature expansion of the effective potential for the Majoron field (see Appendix C for a brief overview). The latter gives a Majoron VEV, $\Phi(T)$, with the same temperature dependence of Eq. (19) and a critical temperature

$$T_c^2 = \frac{12\lambda\Phi_0^2}{2\lambda + \sum_I y_I^2}, \quad (42)$$

where $\Phi_0 \equiv \Phi(T=0)$. We show in Fig. 2 the enhancement of the asymmetry as a function of $M_{N_I}^0/T_c$, obtained by solving Boltzmann equations numerically with the mass profiles that result from Eqs. (17), (19), and (42). As in Fig. 1, we chose $M_1 = M_2/2 = 10^9$ GeV, and used two random choices of Yukawa matrices F (given by Eq. (101) and (102) in Appendix E) with typical real and imaginary parts of 10^{-3} , giving light neutrino masses below ~ 0.2 eV (and thus within an order of magnitude compatible with current cosmological bounds implying $\sum m_\nu < 0.23$ eV [51]). The Yukawa y_1 was fixed at 1, so that the value of λ is given implicitly by Eq. (42) following from the choice of M_I^0/T_c . Fig. 2 illustrates that, as argued before, the asymmetry is

indeed enhanced with growing M_I^0/T_c , saturating at the zero-washout limit given by the upper dashed line. The growth is approximately, although not exactly, linear with the numerical calculations including flavour effects. Since washout can be flavour dependent, it can alter the sign of the asymmetry with respect to its value in the zero washout limit. As a fast second-order phase transition tends to suppress washout effects, the sign of the asymmetry can flip as M_I^0/T_c grows, as seen in the dashed line of Fig. 2. For the solid line, the choice of Yukawa matrix gives no strong flavour effects, washout affects all flavours evenly, and there is no change of sign in the asymmetry.

For $M_I^0/T_c \lesssim 5$, the asymmetry coincides with that in the constant mass limit, given by the dotted lines in Fig. 2. This is because the temperature at the onset of the phase transition is large enough for the N_I to attain near-equilibrium abundances, and so the effect of the phase transition is erased. A sizeable enhancement of the asymmetry from a large departure of equilibrium after the phase transition therefore requires $M_I^0/T_c > 10$. In this analysis, we do not include the effects of scattering or decays of the particle excitations of the Φ field, to which we turn in Sec. 4.

The previous results were obtained using the tree-level potential with the dominant high-temperature corrections. However, as we show in Sec. 5, quantum corrections can spoil the shape of the potential precisely in the region of large M_I^0/T_c , leaving as an open question whether large enhancements of the asymmetry may be realized in realistic scenarios.

3.4 Slowly evolving scalar field

If the N_I masses induced by the symmetry-breaking scalar are time-dependent but very slowly varying, they can be considered constant throughout baryogenesis. Thus there will not be an enhanced departure from equilibrium. However, it does mean that the N_I masses in the early universe are not directly related to their values today. In particular, if we consider the case where the N_I are actual RHNs giving rise to the observed SM neutrino masses, the value of N_I at the time of baryogenesis may not be directly related to the small SM neutrino masses constrained by low-energy neutrino experiments or by the cosmic microwave background. As advocated in Ref. [32], this could in principle allow for exceptions to the Davidson-Ibarra bound on N_I masses that apply for non-resonant, hierarchical leptogenesis scenarios [52]. Such bounds require high reheat temperatures after inflation ($\gtrsim 10^9$ GeV), which can be problematic in models with new, super-weakly coupled low-mass degrees of freedom: for example, high reheat temperatures in supersymmetric models can imply a cosmologically disfavoured over-abundance of gravitinos [53].

To understand whether a relaxation of the Davidson-Ibarra bound is permitted in models with slowly varying N_I mass, we first review the origin of the bound, which arises from a relation between the CP -violating sources of the asymmetry, ε_I^α , and the light SM neutrino masses. The physical reason for the bound is that, in the hierarchical limit and absent any cancellations in matrix products, ε_1^α is proportional to the square of the Yukawa matrix $F_{\alpha I}$ as seen in Eq. (2). Since the typical scale of the Yukawa couplings is $F^2 \sim m_\nu M_1/v^2$, smaller RHN masses gives a smaller source for the asymmetry. Quantitatively, one starts with Eq. (2), and using the usual see-saw relation between the SM neutrino masses, RH neutrino masses, and Yukawa couplings, one obtains

$$m_{IJ}^\nu \approx \sum_K \frac{v^2}{M_K} F_{IK} F_{JK}, \quad (43)$$

where v is the Higgs VEV. The Davidson-Ibarra bound applies in the hierarchical limit where leptogenesis is dominated by N_1 . For $x_{J1} = M_J^2/M_1^2 \gg 1$ in Eq. (2), the CP -violating source due to the decays of N_1 is [52]

$$\varepsilon_1^\alpha \approx \frac{3M_1}{16\pi v^2 (F^\dagger F)_{11}} \text{Im}[F_{\alpha 1} (m^\nu F)_{\alpha 1}]. \quad (44)$$

This expression demonstrates that, for fixed SM neutrino masses m_{IJ}^ν and a lower bound on ε_1^α from the requirement of successful baryogenesis, there exists a lower bound for M_1 .

We now turn to how leptogenesis is affected in models where the M_I were different in the early universe than today. The simplest way to see that the CP -violating source is time independent is by referring to the original formulation in Eq. (2). There, the N_I masses only appear in the ratio M_J^2/M_I^2 , and hence a universal

scaling of all Majorana masses in the early universe results does not change ε_1^α . In Eq. (44), the same result holds due to the fact that the re-scaling of M_1 in the early universe is exactly compensated by the scaling of m^ν . Therefore, the CP -violating source is time independent, in contradiction with the claim of Ref. [32].

The most important effect of a different mass for N_I in the early universe is on the efficacy of washout processes. Recall that the dimensionless washout factor is

$$\mathcal{K}_1^\alpha = \frac{\Gamma_{N_1} \text{Br}(N_1 \rightarrow \alpha)}{H(M_1)}. \quad (45)$$

Considering only the scaling due to mass, the width varies linearly with M_1 while the Hubble scale evaluated at $T = M_1$ varies quadratically with M_1 in a radiation-dominated universe. We therefore have for constant Yukawa couplings and varying mass,

$$\mathcal{K}_1^\alpha \propto \frac{1}{M_1}. \quad (46)$$

In turn, we have that the asymmetry in the strong washout regime is $Y_{\Delta L_\alpha} \sim 1/\mathcal{K}_1^\alpha$, and so

$$Y_{\Delta L_\alpha} \propto M_1. \quad (47)$$

To summarize, for N_1 in the strong washout limit, a larger value for M_1 in the early universe results in a linear enhancement of the lepton asymmetry with the N_1 mass.

For M_1 that is sufficiently large, $\mathcal{K}_1^\alpha \lesssim 1$ and leptogenesis occurs instead in the weak washout limit. Here, the asymmetry is proportional simply to $\varepsilon_1^\alpha Y_{N_1}(0)$, see Eq. (8). In the weak washout limit, the asymmetry is sensitive to the primordial N_1 abundance since scattering with SM leptons is insufficient to establish an equilibrium abundance. If some other particle couples to N_1 at $T \gg M_1$ such that it comes into thermal equilibrium, then $Y_{N_1}(0) = Y_{N_1}^{\text{eq}}$. Since both ε_1^α and $Y_{N_1}(0)$ are independent of the early-universe value of M_1 , then the asymmetry no longer changes with respect to M_1 . If instead the Yukawa couplings between N_1 and L_α provide the dominant interactions of N_1 , then the abundance of N_1 at the time it begins decaying is completely determined by the Yukawa couplings, and hence \mathcal{K}_1^α . For smaller \mathcal{K}_1^α , fewer N_1 exist and can decay to produce an asymmetry. Therefore, we find that there is a maximum value of M_1 in the early universe corresponding to $\mathcal{K}_1^\alpha \approx 1$, and for larger M_1 , the abundance at the time of decay drops and the asymmetry decreases once again.

To verify this behaviour, we consider a concrete 3×2 flavour scenario where we fix the zero-temperature N_I mass, M_I^0 , and vary its mass at the time of leptogenesis. We use $M_1^0 = 10^9$ GeV, $M_2^0 = 2 \times 10^9$ GeV, and a randomly generated Yukawa matrix, Eq. (101)), giving rise to SM neutrino masses compatible with cosmological bounds. We then solve the Boltzmann equations numerically. We show the results in Fig. 3, and the figure clearly shows the linear dependence of the asymmetry with M_1 in the strong washout regime, its flattening at large M_1 if we assume a primordial equilibrium abundance, and its turnover and decrease at large M_1 if we assume the abundance originates only from scattering with SM leptons.

To conclude this discussion, we note that for SM neutrino masses consistent with the Planck cosmological bound $\sum_i m_i^\nu < 0.23$ eV [51], and with recent fits to oscillation data yielding a largest mass difference of the order of 0.05 eV [54], the ratio $\Gamma_{N_1} \text{Br}(N_1 \rightarrow \alpha)/H(M_1^0) \gg 1$, which corresponds to the strong washout regime. This can be easily seen by substituting these numerical values into Eq. (43) and Eq. (15). In the strong washout regime, an enhancement of the asymmetry requires larger Majorana masses in the early universe, $M_I > M_I^0$, which can arise if the symmetry-breaking scalar field rolls down from large to small field values. If leptogenesis occurs from a thermal abundance of N_I , then the asymmetry-enhanced scenario requires a larger reheat temperature than in conventional leptogenesis to populate the N_I particles. This contradicts the conclusion of Ref. [32].

4 Asymmetry Damping from New Annihilation Modes

To this point, we have considered the effects of a time-dependent particle mass on the asymmetry generated from its decays. Realistically, such a time-varying mass originates from the dynamics of some scalar field(s),

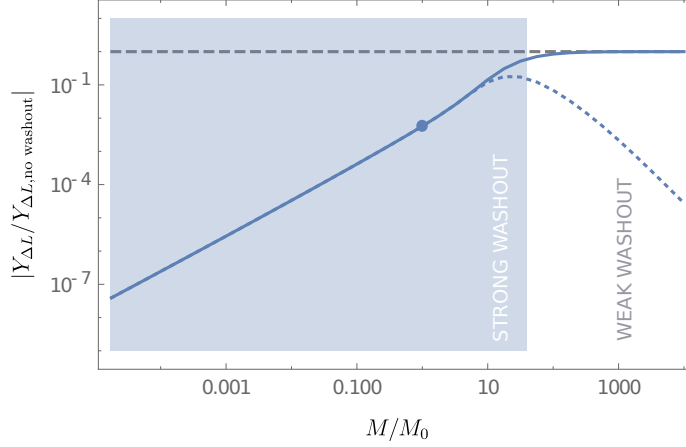


Figure 3: Lepton asymmetry under a **universal rescaling** of the RHN masses (M_I) in the early universe relative to today. The zero-temperature masses are $M_{N_1}^0 = 10^9$ GeV, $M_{N_2}^0 = 2 \times 10^9$ GeV, and we use a random Yukawa matrix with typical real and imaginary parts of $O(10^{-3})$, see Eq. (101). The horizontal dashed line corresponds to the maximum possible asymmetry (achieved with zero washout and initial equilibrium abundances for the N_I). The blue lines include washout effects: the solid line corresponds to initial equilibrium abundances for the N_I , and the dashed blue line corresponding to zero initial abundances. The blue dot corresponds to no difference between the M_I in the early universe and the present. The shaded blue region delimits the strong washout regime, $\mathcal{K}_I^\alpha > 1$ for some flavours I, α .

Φ , breaking the $B - L$ symmetry. In realistic models, some or all of the components of Φ may have masses comparable or below the typical momentum scale of interactions in the plasma at the time of leptogenesis, and it is therefore important to consider the effects of N_I interactions with Φ particles in determining the final lepton asymmetry. Such effects have been considered in Refs. [28, 29], although our work additionally combines the effects of the time varying parent-particle mass with the effects of scattering between N_I and Φ .

The Yukawa interaction between N_I and Φ (henceforth called the Majoron) as specified in Eq. (16) leads to an irreducible scattering process $N_I \bar{N}_I \rightarrow \Phi^\dagger \Phi$ that can change the number density of N_I . This process is shown in the left pane of Fig. 4. Additionally, the scalar potential in the broken phase typically contains cubic couplings of the scalar field components, and these lead to $N_I N_I \rightarrow \Phi \Phi$ scattering indicated by the diagram in the right pane of Fig. 4. It is important to include these scattering processes in the Boltzmann equations, Eq. (4), whenever $M_\Phi \leq M_I$.

We now argue that the scattering of N_I into Φ is typically kinematically accessible and important if Φ is a complex scalar that breaks a continuous global symmetry, and if the conditions for asymmetry enhancement due to a “fast” second-order phase transition are realized (as outlined in Section 3.3). Let us first assume that Φ is a complex field breaking a continuous global symmetry. There is at least one massless Goldstone mode, φ , in the broken phase and so N_I annihilation into the Goldstone fields is always kinematically accessible. The only way that this process could be unimportant is if the Yukawa couplings, y_I , are all small. However, we have seen that a substantial modification of the asymmetry in a second-order phase transition requires

$$\frac{M_I(T=0)}{T_c} = \frac{y_I \Phi_0}{T_c} \gg 1. \quad (48)$$

Thus, the only way that y_I can be small is if $\Phi_0 \gg T_c$. However, as we show in Section 5, it is challenging to obtain large hierarchies in Φ_0/T_c , and so achieving $M_I^0/T_c \gg 1$ typically requires large y_I . We therefore find it likely that annihilations into at least some components of Φ are important during leptogenesis. Possible exceptions to this argument include scenarios with a discrete, rather than global, symmetry of a multi-field model; however, we still find that the requirement of a delayed phase transition typically leads to a relatively flat direction in the potential, which in turn suggests the existence of low-mass scalars to which N_I can

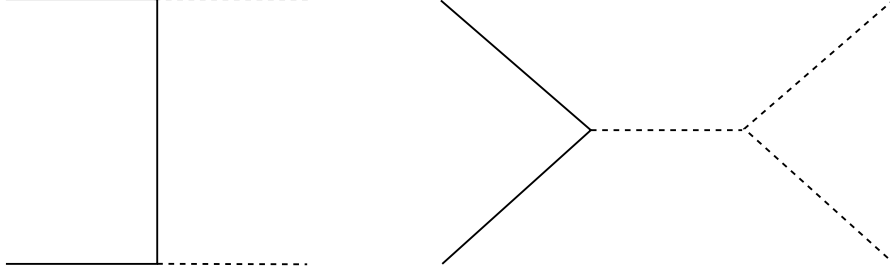


Figure 4: Annihilation diagrams of the RHNs (solid lines) into scalars (dashed lines).

annihilate.

The effect of annihilations and their inverse processes was systematically studied in Ref. [29] in the scenario with a time-independent N_I mass. In that work, it was pointed out that annihilations have two effects. First, when the N_I are weakly coupled to the thermal bath and cannot otherwise reach a thermal abundance (such as in the weak washout regime), inverse annihilations open up new channels of production that increase the N_I population and can enhance the asymmetry. On the other hand, once the N_I can reach a thermal distribution at high temperatures, the generic effect of annihilations is to provide a lepton-number-preserving mode to relax the N_I abundance to its equilibrium value, decreasing the asymmetry resulting from decays⁴. As we have done throughout our paper, we concentrate on the strong washout regime where the effects of a time-varying mass are most pronounced.

4.1 Boltzmann Equations with Annihilations

In the presence of new annihilation modes $N_I N_I \rightarrow \phi\phi$ (where ϕ stands in for any of the scalar components of Φ), the Boltzmann equation for the N_I number density is

$$\frac{dY_{N_I}}{dt} = -\langle\Gamma_{N_I}\rangle (Y_{N_I} - Y_{N_I}^{\text{eq}}) - 2s(z)\langle\sigma_{N_I N_I \rightarrow \phi\phi}v\rangle \left[Y_{N_I}^2 - (Y_{N_I}^{\text{eq}})^2 \right]. \quad (49)$$

We use the convention where the thermally averaged cross section includes a symmetry factor of $1/2$ for identical initial states. Because the N_I obtain their masses from the same y_I couplings that mediate the annihilation terms, we need only concern ourselves with on-diagonal annihilations. Assuming $Y_{N_I} \approx Y_{N_I}^{\text{eq}}$ (as is true in the strong washout regime and before inverse processes decouple), we can define a rate

$$\Gamma_I^{\text{ann}} \equiv 4\langle\sigma_{N_I N_I \rightarrow \phi\phi}v\rangle s(z) Y_{N_I}^{\text{eq}}. \quad (50)$$

In this limit, we have

$$\frac{dY_{N_I}}{dt} \approx -[\langle\Gamma_{N_I}\rangle + \Gamma_I^{\text{ann}}] (Y_{N_I} - Y_{N_I}^{\text{eq}}). \quad (51)$$

It is clear that, if $\Gamma_I^{\text{ann}} \gtrsim \langle\Gamma_{N_I}\rangle$, then the change in N_I abundance is dominated by annihilations, and it is important to include the annihilation term when solving the Boltzmann equations.

The effects of annihilations on the lepton asymmetry can be found by substituting Eq. (51) into the Boltzmann equation for $Y_{\Delta L\alpha}$, namely the second line in Eq. (4). We then have as our equation for the asymmetry, $Y_{\Delta L\alpha}$,

$$\frac{dY_{\Delta L\alpha}}{dt} = -\sum_I \varepsilon_I^\alpha \frac{\langle\Gamma_{N_I}\rangle \text{Br}(N_I \rightarrow \alpha)}{\langle\Gamma_{N_I}\rangle + \Gamma_I^{\text{ann}}} \frac{dY_{N_I}}{dt} - \Gamma_W^\alpha Y_{\Delta L\alpha}, \quad (52)$$

⁴Additionally, it may be possible that new modes for asymmetry generation can occur via Φ interactions with SM fields. This is highly model-dependent, however, and in the simplest scenario where Φ decays to SM fields via a small mixing with the SM Higgs, Φ effectively carries no baryon or lepton number.

where again Γ_W^α is the washout rate. The solution to this equation has an integral form analogous to Eq. (6). Based on our earlier arguments, we know that the asymmetry is predominantly generated for times $t > t_*$, where $\Gamma_W^\alpha(t_*) = H(t_*)$. We can identify two limits of the solution, depending on the relative magnitudes of $\langle \Gamma_{N_I} \rangle$ and Γ_I^{ann} at t_* :

1. If $\langle \Gamma_{N_I} \rangle(t_*) > \Gamma_I^{\text{ann}}(t_*)$, then annihilations are subdominant to decays, and the full Boltzmann equation, Eq. (52), reduces to the simpler case with no annihilations included and the asymmetry is the same as before.
2. If $\langle \Gamma_{N_I} \rangle(t_*) < \Gamma_I^{\text{ann}}(t_*)$, then we see that the lepton asymmetry is not efficiently produced because most of the N_I disappear via annihilation into ϕ instead of decays into L_α . We expect that the resulting lepton number asymmetry is approximately suppressed by the ratio $\langle \Gamma_{N_I} \rangle(t_*)/\Gamma_I^{\text{ann}}(t_*)$. Often, it is said that “ N_I is kept more in equilibrium” by the annihilation processes.

It should be noted that $\Gamma_I^{\text{ann}} \propto Y_{N_I}^{\text{eq}}$, and so the annihilation rate decreases exponentially as a function of time for $T \ll M_I$ (as is familiar, for example, from the thermal freeze-out of dark matter annihilations). Consequently, the annihilations play less of a role in determining the final lepton asymmetry for a later decoupling of washout.

Broadly speaking, the above arguments only apply to individual flavours. There is always the possibility of nontrivial flavour effects which could, for instance, enhance the total asymmetry in the presence of annihilations. For example, one can consider a situation with weak washout in which the sum of CP -violating sources is zero due to some lepton flavour symmetries, and the total asymmetry would vanish due to a cancellation of the asymmetries in different flavours. If annihilation rates are not flavour-universal, then the flavoured asymmetries would be suppressed by different factors, the cancellation would be spoiled and a net asymmetry would arise.

4.2 Analytic Estimate of Annihilation Rates

In order to understand when annihilations might be important for the lepton asymmetry, we may consider the leading analytic dependence of each of the washout and annihilation rates, as the importance of annihilations depends on their relative size. Considering a model where N_I obtains a mass through interactions with a symmetry-breaking complex scalar as in Eq. (16). In the broken phase, the scalar Φ decomposes into radial and angular modes, $\Phi = (v_\phi + \phi_r)e^{i\phi_i/v_\phi}/\sqrt{2}$. When scalar masses and cubic interactions are small, the annihilation of N_I proceeds mainly through the first family of diagrams in Fig. 4; for simplicity, we consider the annihilation into ϕ_r for our analytic estimates but the full result is not qualitatively different. This annihilation rate of N_I into two scalars is velocity suppressed due to the negative intrinsic parity of the initial state of two Majorana fermions. In the small-velocity and small- ϕ_r -mass expansions, we find:

$$\sigma_{N_I N_I \rightarrow \phi_r \phi_r}(s) = \frac{3y_I^4 \sqrt{s - 4M_I^2}}{128\pi M_I^3} + \mathcal{O}(s - 4M_I^2)^{3/2}, \quad (53)$$

and the full result is given in Appendix D. To find Γ_I^{ann} , we must compute the thermally averaged cross section. This involves an integration over s with an exponentially suppressed weight for $M_I/T \gg 1$ (as seen in Appendix B), and so it is permissible to evaluate the integral using the velocity expansion. The result in the $M_I/T \gg 1$ limit is

$$\Gamma_I^{\text{ann}} \approx \frac{9\sqrt{2}y_I^4 T^{5/2}}{128\pi^{5/2} M_I^{3/2}} e^{-M_I/T}. \quad (54)$$

This can now be compared with the decay rate.

For $T \ll M_I$, the thermal averaging has no effect on the width of N_I (see Appendix B), and so we can simply use the zero-temperature width from Eq. (14),

$$\Gamma_{N_I} = \frac{(F^\dagger F)_{II} M_I}{8\pi}. \quad (55)$$

Taking the ratio then gives

$$\frac{\Gamma_I^{\text{ann}}}{\langle \Gamma_{N_I} \rangle} \sim \frac{9\sqrt{2} y_I^4}{16\pi^{3/2} (F^\dagger F)_{II}} z_I^{-5/2} e^{-z_I}, \quad (56)$$

where we use the usual dimensionless quantity $z_I \equiv M_I/T$. The time at which annihilations become subdominant to decays, z_I^a , is defined implicitly by $\Gamma_I^{\text{ann}}(z_I^a)/\Gamma_{N_I}(z_I^a) \equiv 1$.

We need to evaluate Eq. (56) at the time when washout interactions decouple. Let us consider for simplicity the single-flavour limit, in which the N_I have a hierarchical spectrum such that only annihilations and decays of N_1 are relevant. Using Eqs. (7) and (14), we have

$$\frac{\Gamma_W^\alpha(T)}{H(T)} \sim \frac{\sqrt{\pi} \mathcal{K}_1^\alpha}{4\sqrt{2}} z_1^{7/2} e^{-z_1}. \quad (57)$$

The condition that $\Gamma_W^\alpha(z_1^*)/H(z_1^*) = 1$ defines a time z_1^* .

We can compare the time at which annihilations become subdominant to decays, z_1^a , to the time at which washout decouples, z_1^* . In particular, let us consider the case of SM neutrino masses generated using a simple see-saw mechanism. Using the see-saw relations, the Yukawa couplings $F \sim (m^\nu M_1/v^2)^{1/2}$ and $m^\nu \approx 0.1$ eV, it is straightforward to use Eqs. (56) and (57) to find that $z_1^* = z_1^a$ for $M_1 \sim 10^6 - 10^7$ GeV. For higher N_1 masses, the Yukawa couplings are large enough that the decay dominates over annihilations at z_1^* , and so annihilations are not important during the epoch of asymmetry generation. By contrast, for lower masses the Yukawa couplings are small enough that annihilations are important during asymmetry generation and suppress the efficacy of leptogenesis. In the most conventional regime of hierarchical leptogenesis in models satisfying the Davidson-Ibarra bound [52], annihilations are never important. These overall conclusions can be different in models where the Yukawa couplings are much larger than the naïve expectation due to cancellations among entries [55]: in this case, F is larger than expected and annihilations play less of a role than in the naïve see-saw.

For non-hierarchical N_I , one expects the individual washout rates to be comparable. Given the stronger overall washout at late times for a given value of M_1 , washout processes tend to decouple at later times for a degenerate spectrum, and so one expects that annihilations can have a somewhat smaller effect than in hierarchical scenarios with a similar value of M_1 . The only way to determine precisely whether they are important is to calculate the relative annihilation, decay, and washout rates considering all flavours and see which processes decouple first.

We now turn to the question of how the above arguments change in the presence of a time-dependent mass. Specifically, we are most interested in how annihilations can affect the asymmetry with a second-order phase transition, as we saw in Section 3.3 that this was the type of phase transition that could lead to an enhanced asymmetry. The effect of the second-order phase transition is to make the time of washout freeze-out earlier, because the mass is changing with a rate faster than the characteristic Hubble expansion. However, we see that making z_1^* occur earlier only leads to an increase in the asymmetry provided $z_1^a < z_1^*$; otherwise, the N_1 abundance is damped by annihilations and the resulting asymmetry is not as enhanced as would otherwise have been anticipated. We see, therefore, that the annihilations of N_I into ϕ tend to decrease the enhancement associated with a second-order phase transition.

4.3 Numerical Analysis

To illustrate the previously discussed features, we perform a numerical analysis including the effects of annihilations. We consider a 3×2 flavour system, with two values of Yukawa couplings to the Majoron ($y_1 = 1$ or $y_1 = 0.3$), and including the full cross sections for the annihilation of N_I into all the Majoron's components, both in the broken and unbroken phases. We provide details of the calculation in Appendix D.

Time-Independent Masses: First we consider the case where the VEV of Φ is time-independent, and we assume equilibrium boundary conditions at $T = 100M_1$. Starting from a randomly generated Yukawa matrix F_7 (given by Eq. (103) in Appendix E) which gives SM neutrino masses $m^\nu \lesssim 0.2$ eV for $M_1 = 10^7$ GeV, we vary M_1 , and make two different choices for $F_{\alpha I}$: either $F = \sqrt{M_1/10^7 \text{ GeV}} F_7$, which keeps m^ν constant, or

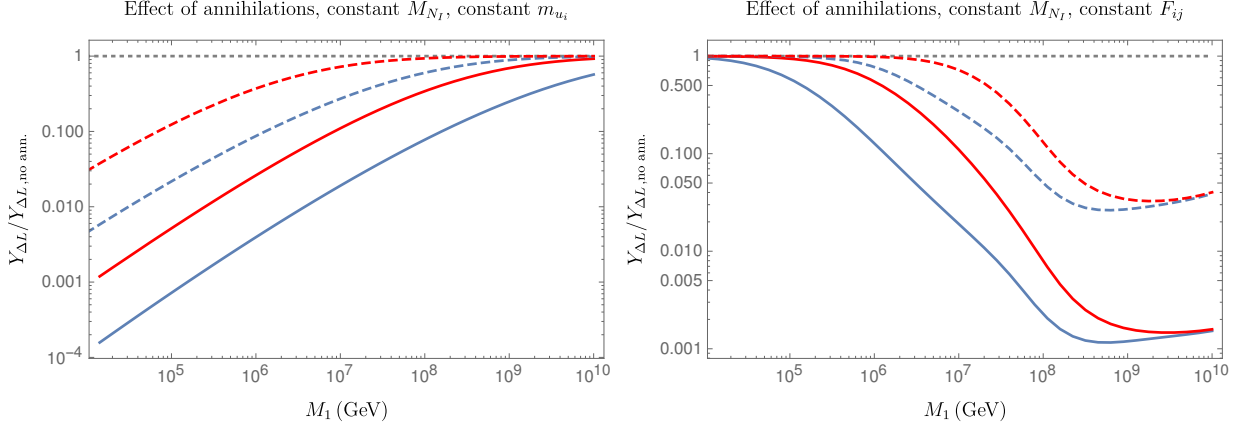


Figure 5: Ratio of the total lepton asymmetry **including annihilations vs. without annihilations**, plotted as a function of M_1 . We consider time-independent M_I , two flavours of N_I and three flavours of L_α . On the left plot, the leptonic Yukawa couplings $F_{\alpha I}$ are rescaled under changes of M_1 to keep the masses of the SM ν particles constant and $\lesssim 0.2$ eV. On the right plot, we kept $F_{\alpha I}$ constant as described in the text. We assumed either $M_2 = 2M_1$ (hierarchical scenario, blue lines) or $(M_2 - M_1)/M_1 = 10^{-6}$ (resonant scenario, red lines). Solid lines correspond to $y_1 = 1$, and dashed coloured lines to $y_1 = 0.3$.

$F = F_7$. The masses of the scalars are taken to be zero (corresponding to negligible self-interactions of the scalar).

Our results for the variation of the asymmetry as a function of M_1 and for our choice of F_7 are shown in Fig. 5. In all cases, the effects of annihilations are less pronounced for $y_1 = 0.3$ (dashed coloured lines) than for $y = 1$ (solid lines). Also, as anticipated earlier annihilations are more relevant for a hierarchical spectrum (blue lines, with $M_2 = 2M_1$), than for a degenerate one (red lines, with $(M_2 - M_1)/M_1 = 10^{-6}$). This is due to the larger washout rate in the degenerate case.

In the left pane of Fig. 5, we show the results for the scenario in which M_1 and F are correlated to preserve the see-saw relation, which in turn affects the degree to which annihilations are important relative to decays. For smaller M_1 , we see that annihilations are more important due to the smaller couplings F , and consequently the asymmetry is suppressed at these smaller masses.

In the right pane of Fig. 5, the lepton Yukawa couplings F are kept at a constant value. In this case, increasing M_1 makes the washout weaker in relative terms according to Eq. (46) and (57) so that washout decoupling happens at earlier times. This increases the range of temperatures at which annihilations can affect the asymmetry, and thus they more dramatically suppress the asymmetry. The asymmetry suppression becomes maximal when washout becomes irrelevant for all $T \lesssim M_1$, in which case the asymmetry is purely determined by the moment in which annihilations become subdominant with respect to decays; the corresponding value of z_1^a does not depend on M_1 for constant F (see Eq. (56)) and thus the curves in the right pane of Fig. 5 become flat.

Time-Dependent Masses: We now turn to the case in which the VEV of the Majoron Φ and the associated particle masses are temperature dependent as a consequence of a second-order phase transition. As in Section 3.3, we focus on the model of a single symmetry-breaking scalar with the interactions of Eq. (41), and use the values for the Majoron VEV and the particle masses in the high-temperature expansion from Eq. (17), (19), and (42), as well as the results for the scalar masses in Appendix C.1. For computing the thermally averaged annihilation cross sections, we distinguish the broken and unbroken phases, with the zero-temperature cross sections given in Appendices D.1 and D.2, respectively. The thermally averaged cross section, calculated as detailed in Appendix B, diverges at the critical temperature when the RHNs and scalars are massless. This divergence is regularized by a resummation of thermal contributions to the N_I propagator. However, leptogenesis occurs for $T < M_I(T)$, in which case the thermal contributions to N_I propagation are subdominant

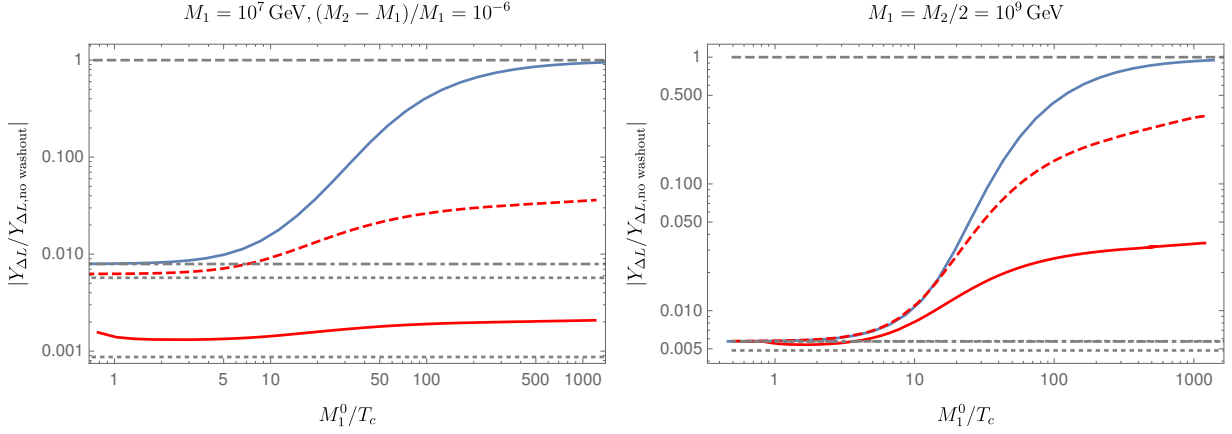


Figure 6: Ratio of the total lepton asymmetry vs. its value in the zero washout limit, plotted as a function of M_I^0/T_c , for two flavours of N_I and three flavours of L_α . For the left pane, $M_1 = 10^7$ GeV, $(M_2 - M_1)/M_1 = 10^{-6}$, while on the right pane $M_1 = M_2/2 = 10^9$ GeV. The leptonic Yukawa couplings $F_{\alpha I}$ are randomly generated and constrained to give SM neutrino masses $\lesssim 0.2$ eV. The solid blue lines neglect annihilations, while we include annihilations in the red lines with $y_1 = 1$ (solid red), and $y_1 = 0.3$ (dashed red). The horizontal lines represent, from top to bottom, the zero washout limit in the absence of annihilations, followed by the constant mass limits for the case without annihilations for $y_1 = 0.3$ and $y_1 = 1$.

to the tree-level mass and can be neglected.

We show the results of the numerical calculations in Fig. 6. On the left pane, we consider a degenerate spectrum, with $M_1 = 10^7$ GeV, $(M_2 - M_1)/M_1 = 10^{-6}$, while in the right pane we have $M_1 = M_2/2 = 10^9$ GeV. In both cases we use randomly generated Yukawa matrices consistent with SM neutrino masses and given in Eq. (103) (left pane) and Eq. (101) (right pane) in appendix E. The matrices have the property that the asymmetry for a time-independent mass and negligible annihilations has the same sign regardless of whether or not washout processes are active (when neglecting annihilations, the asymmetry has the behaviour of the solid line in figure 2). The solid blue lines give the behaviour of the asymmetry when annihilations are neglected, and the red lines include the effect of annihilations for $y_1 = 1$ (solid red), and $y_1 = 0.3$ (dashed red). The horizontal lines represent, from top to bottom, the zero washout limit without annihilations, and then the constant mass limits for the case without annihilations, for $y_1 = 0.3$, and for $y_1 = 1$. Note that annihilations thwart the enhancement of the asymmetry due to the second-order phase transition, the effect being more pronounced for larger y_I and lower M_1 .

5 Realistic Phase Transitions and Baryogenesis

In the previous sections, we have found that the baryon asymmetry resulting from the out-of-equilibrium decay of a particle N_I can be affected by a phase transition in its mass, M_I . In particular, we found that an enhancement of the asymmetry is possible in models with fast second-order phase transitions, while the asymmetry may suffer a suppression due to additional annihilation modes. The baryon asymmetry was calculated assuming a particular time-dependent mass profile for N_I and, in particular, taking the zero-temperature mass, M_I^0 , and critical temperature, T_c , as free parameters. We found that for second-order phase transitions to give a substantial enhancement of the baryon asymmetry, it was necessary to have $M_I^0/T_c \gtrsim 10$ (see Fig. 2).

We now turn to addressing the question of how such time-dependent mass profiles can be obtained in realistic, perturbative models of spontaneous symmetry breaking. As we show below, the large value of $M_I^0/T_c \gg 1$ needed for an appreciable enhancement of the asymmetry is not a generic feature of scalar potentials and only results from tuned parameters in the potential which can be destabilized by quantum corrections. Below, we first consider the case of symmetry breaking in single-scalar models in Section 5.1.

Noting that symmetry breaking patterns can be substantially different in multi-field models, we then study two-field models in Section 5.2.

5.1 Single-Field Models

The simplest model of N_I achieving a mass through spontaneous symmetry breaking is if the symmetry-breaking sector consists of a single scalar field, Φ , which is the Majoron. The tree-level potential was given in Eq. (41):

$$\mathcal{L}_{\text{mass}} \supset -\frac{y_I}{2} \Phi \bar{N}_I^c N_I + \text{h.c.} + m_\Phi^2 \Phi^\dagger \Phi - \frac{\lambda}{4} (\Phi^\dagger \Phi)^2. \quad (58)$$

This tree-level potential is corrected by finite-density effects in the early universe. If we consider only the leading T^2 terms in the finite-temperature potential resulting from a high-temperature expansion (see Appendix C), the relation between zero-temperature N_I mass and Φ VEV is:

$$\frac{M_I^0}{T_c} = \frac{y_I^2}{12\lambda} \left(2\lambda + \sum_J y_J^2 \right). \quad (59)$$

This result suggests that, in order to achieve $M_I^0/T_c \gg 1$, one needs $y_I^4 \gg \lambda$ for at least one flavour N_I . This limit is problematic: for example, radiative corrections to the Φ quartic coupling from loops of N_I scale like y_I^4 , and so in this limit radiative corrections can dominate over the tree-level contributions to the potential. This suggests, at the very least, the necessity of a cancellation between tree- and loop-induced contributions to the potential that realize the relation $y_I^4 \gg \lambda$ for the renormalized couplings.

In reality, the situation is worse than a fine tuning of parameters. The reason is that the renormalized quartic coupling can be small at only a single scale as a result of fine tuning. Renormalization group (RG) effects modify the quartic coupling at other scales in the potential, and large Yukawa couplings y_I can destabilize the minimum of the potential under RG evolution. This effect is, for example, well-appreciated in the SM and has received renewed interest with the recent measurements of the Higgs boson and top quark masses [56, 57]; in our case, the computation is simpler because we do not need to concern ourselves with questions of gauge invariance in the effective potential and tunnelling calculations [58, 59].

To account for these effects, we compute the RG-improved effective potential with the RG scale set to a VEV-dependent quantity. In order to minimize logarithmic corrections, the former can be chosen as the largest particle mass in the Φ background [60], which for $\mathcal{O}(1)$ couplings coincides with $|\Phi|$. Choosing then $\mu = |\Phi|$, in the limit of large field values the quartic coupling becomes

$$V_4 = \frac{\lambda_{\text{eff}}(|\Phi|)}{4} (\Phi^\dagger \Phi)^2, \quad (60)$$

$$|\Phi| \frac{\partial \lambda_{\text{eff}}(|\Phi|)}{\partial |\Phi|} \equiv \beta_\lambda(|\Phi|) = -\frac{1}{4\pi^2} \sum_I y_I^4 + \mathcal{O}(\lambda y_I^2). \quad (61)$$

For a reference scale μ_0 , the effective quartic coupling can be approximated as,

$$\lambda_{\text{eff}}(|\Phi|) = \lambda(\mu_0) + \beta_\lambda \log \frac{|\Phi|}{\mu_0}, \quad (62)$$

which can also be directly derived from the large-field expansion of the Coleman-Weinberg potential, Eq. (80), in Appendix C. For y_I not too large with respect to λ , the effect of $\beta_\lambda < 0$ is to make the potential negative at large field values where $\lambda_{\text{eff}}(|\Phi|)$ crosses zero. The result is a local, metastable minimum for Φ at small field values, and a global minimum at large field values, much like in the metastable case of the SM Higgs potential. This is not necessarily a problem, as quantum tunnelling and thermal transitions to the unstable region are typically extremely suppressed if it happens at sufficiently large field values. Even if the origin/zero-temperature metastable “vacuum” are not the true minima of the potential for any T , the presence of the

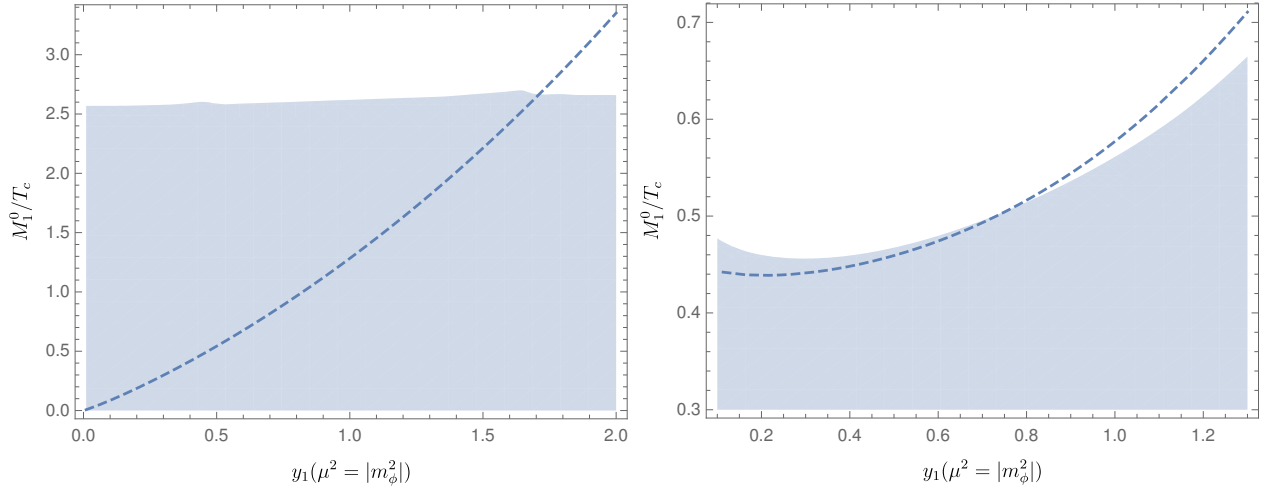


Figure 7: Allowed regions for M_I^0/T_c in single-scalar models with degenerate N_I and a constant zero-temperature VEV $\langle\Phi\rangle$. The shaded regions show allowed parameters with the RG-improved full one-loop effective potential (including thermal Daisy resummation [62]), while the dashed lines show the relationship between M_I^0/T_c and y_I obtained with the effective potential ignoring zero-temperature loop corrections and keeping only terms in the high- T expansion. Left pane: upper bounds found by demanding the existence of a local metastable minimum at field values $\sim m_\Phi$, and zero-temperature VEV $\langle\Phi\rangle \sim 6 \times 10^9$ GeV. Right pane: upper bounds obtained by demanding stability of the scalar potential up to the Planck scale, and zero-temperature VEV $\langle\Phi\rangle \sim 0.7 \times 10^9$ GeV.

distant true vacuum can be irrelevant, with baryogenesis proceeding as expected and the metastable vacuum surviving throughout the history of the Universe⁵.

For larger tree-level values of y_I^4/λ , $\lambda_{\text{eff}}(|\Phi|)$ becomes negative even for values of $|\Phi| \sim m_\Phi$ and the effective potential may not have a local minimum in the vicinity of m_Φ at all. Since according to Eq. (59) this is the coupling regime expected to give large M_I^0/T_c , we expect that an upper bound on M_I^0/T_c may be derived from the requirement of the existence of a local minimum of the potential near m_Φ at zero temperature. We do this by selecting a set of Yukawa couplings, y_I , and finding the value of the quartic couplings, λ , at which the metastable vacuum disappears. This corresponds to a maximum value of M_I^0/T_c .

In the left pane of Fig. 7, we show the upper bound on M_I^0/T_c for the single-scalar model of Eq. (41) as a function of the Yukawa couplings, y_I . For simplicity, we present the results for a quasi-degenerate spectrum of N_I , so that all of the y_I are set equal to one another, although similar results hold for hierarchical spectra. To hold the zero-temperature VEV fixed, we set $m_\Phi^2(\mu = m_\Phi^2) = y_I^4(5 \times 10^8)^2 \text{ GeV}^2$, which gives an approximately y_I -independent value of $\langle\Phi\rangle \sim 6 \times 10^9$ GeV in the metastable vacuum (when it exists). The shaded area on the plot shows the bound obtained from the full one-loop potential with thermal corrections including a Daisy resummation (see Appendix C) [62]. For comparison, we show with the dashed line the point at which the zero-temperature metastable vacuum disappears in the high-temperature expansion and ignoring any zero-temperature quantum corrections; as is evident, this approximation fails to give the correct upper bound for large values of the Yukawa coupling where higher-order corrections are important to include.

A stricter upper bound on M_I^0/T_c can be obtained by requiring a positive effective quartic up to field values of order the Planck scale (*i.e.*, up to $M_P = m_P/\sqrt{8\pi} \approx 2.4 \times 10^{18}$ GeV). This gives a minimum value of λ ensuring stability, λ_{min} . Assuming $m_\Phi^2 = \lambda_{\text{min}}(5 \times 10^8)^2 \text{ GeV}^2$, which gives a y_I -independent local VEV around 0.7×10^9 GeV, the ensuing bound on $M_{N_1}^0/T_c$ is illustrated on the right plot of figure 7. The high-temperature

⁵The suppressed quantum and thermal tunnelling out of the metastable vacuum are again analogous to those of the Higgs' electroweak vacuum in the SM [56]. Although the existence of the unstable region could be problematic during inflation, due to enhanced quantum of light fields fluctuations in the presence of curvature, the field can be stabilized with nonminimal gravitational interactions that enhance the effective mass in the presence of curvature [61].

approximation works much better at deriving this bound because the requirement of stability up to the Planck scale requires that zero-temperature quantum corrections remain suppressed near the metastable vacuum. For a second-order phase transition to a local minimum with $\langle\Phi\rangle \sim m_\Phi$, the high-temperature expansion for all background-dependent masses is expected to give reasonably accurate results.

Even in the most optimistic case in which the local vacuum is not separated from the unstable region by a barrier (as illustrated in the left pane of Fig. 7), it is clear that the allowed values of M_I^0/T_c are far from the regime in which one expects an enhanced baryon asymmetry due to a rapid transition, $M_I^0/T_c \gtrsim 10$. Are there any scenarios in which this conclusion may be evaded? One may expect that larger values of M_I^0/T_c could be allowed in theories where radiative corrections are suppressed or cancel among different fields, as is typical in supersymmetric models. For example, if we consider a potential containing additional scalars S possessing mixed quartic couplings to Φ , then loops of S give positive contributions to the running of λ that cancel the running due to the Yukawa couplings, y_I . An exact cancellation is expected in a models where the various couplings are related by supersymmetry. However, such a scenario poses a new problem: the new couplings of the bosons S to Φ induce a non-analytic cubic term in the effective potential, resulting in a thermal barrier between the origin and the metastable vacuum (see Appendix C):

$$V^T(\Phi) \supset -\frac{T}{12\pi}(m_S^2(\Phi))^{3/2}. \quad (63)$$

With such a barrier, the phase transition to the broken vacuum will be first order, rather than second order. As argued in Section 3.2, first-order phase-transitions with large $\langle\Phi\rangle/T_c$ strongly inhibit, rather than enhance, the production of a baryon asymmetry through N_I decays.

An exception to the above reasoning is if the Φ -dependent terms in Eq. (63) are subdominant to the Φ -independent terms in Eq. (63) for Φ values near the metastable vacuum. This occurs if, for instance, S has a large tree-level mass, $m_S^2 \gg \lambda_{S\Phi}\langle\Phi\rangle^2$, where $\lambda_{S\Phi}$ is the mixed quartic coupling between S and Φ . In this limit the thermal corrections can be approximated by even powers of $\Phi^\dagger\Phi$, which generate no barrier:

$$(m_S^2(\Phi))^{3/2} = (m_S^2)^{3/2} \left[1 + \frac{3}{2}\lambda_{S\Phi}\frac{\Phi^\dagger\Phi}{m_S^2} + \frac{3}{8}\lambda_{S\Phi}^2\left(\frac{\Phi^\dagger\Phi}{m_S^2}\right)^2 + \mathcal{O}\left(\frac{\Phi^\dagger\Phi}{m_S^2}\right)^3 \right]. \quad (64)$$

However, physically we know that large values of m_S^2 correspond to a decoupling of S from the spectrum, and the decoupling theorems ensure that the physical result reproduces the single-scalar limit. The inconsistency is found by noting that the earlier results of the S contribution to the effective potential were derived assuming the dominance of $\log\Phi$ terms in the effective quartic coupling λ_{eff} , which cease to dominate the potential when other scales such as m_S^2 becomes large. We have confirmed with numerical calculations in a model with additional complex scalars that, indeed, no sizeable enhancement of M_I^0/T_c is found with respect to the single-scalar case when one requires a second-order phase transition.

In conclusion, models in which the Majoron field, Φ , is the only field undergoing a second-order phase transition do not naturally accommodate large values of M_I^0/T_c . Thus one cannot obtain sizeable enhancements of the baryon asymmetry with respect to the constant-mass case in a single-field model; instead, typical models yield an asymmetry that is at most comparable to that in constant mass models, and may be smaller due to the effects of annihilations.

5.2 Two-Field Models

In the previous section, we assumed that the breaking of the baryon or lepton symmetry was the result of the dynamics of a single scalar field. There is, however, no reason to assume that the breaking of such a symmetry is so simple; in the SM, for example, there exist multiple sources of electroweak symmetry breaking, namely the Higgs scalar and the chiral condensate. In this section, we study the implications of additional symmetry-breaking fields on the phase transition.

In particular, we focus on the scenario of a multi-step phase transition, where the transition to the $\langle\Phi\rangle \neq 0$ vacuum proceeds from another minimum in field-space, rather than from the origin. This results in a qualitatively different dependence of the phase transition temperature, T_c , relative to the single-field case due

to the fact that T_c no longer results directly from the temperature-dependent effective mass of Φ , but rather depends on the temperature at which the two vacua become degenerate and the transition is allowed. In the case of a single-field model, we found that a delayed phase transition (with post-phase-transition mass large compared to T_c) required large couplings to increase the finite-temperature corrections, which in turn led to large radiative corrections that destabilized the minimum. For a multi-field model, parametrically small values of T_c may instead result due to small, zero-temperature energy differences between the minima.

Multi-field transitions have already been studied in the literature [63, 64, 65, 66, 67]. The previous investigations have focused on scalars responsible for the breaking of electroweak symmetry, but the results can be qualitatively applied to the case of two singlets, one of them being the Majoron, Φ , responsible for breaking baryon or lepton number. We therefore consider a two-field model consisting of Φ and a real scalar, φ . The Majoron Φ is the only field directly carrying baryon or lepton number, and so it alone couples to the RH neutrinos, N_I , of our simplified model of leptogenesis. The tree-level Lagrangian is

$$\mathcal{L} \supset -\frac{y_I}{2} \Phi \bar{N}_I^c N_I + \text{h.c.} + m_\Phi^2 |\Phi|^2 + \frac{m_\varphi^2}{2} \varphi^2 - \frac{\lambda_\Phi}{4} |\Phi|^4 - \frac{\lambda_\varphi}{4!} \varphi^4 - \frac{\lambda_{\Phi\varphi}}{2} |\Phi|^2 \varphi^2. \quad (65)$$

We are interested in the limit in which there occurs first a phase transition to a vacuum with $(\Phi, \varphi) = (0, v_\varphi)$, which can be either second or first order. This is followed by a second-order phase transition in which Φ acquires a VEV (and φ may or may not have a VEV). At high temperatures, the $(0, v_\varphi)$ vacuum should be preferred over configurations with nonzero Φ , implying that thermal corrections predominate along the Φ axis. This follows naturally from the condition that only Φ couples to the thermal bath of the N_I .

The requirement that the final phase transition is second order implies that there should be no barriers generated between the $(0, v_\varphi)$ minimum and the minimum with nonzero Φ at the time of the transition. In particular, there should exist no tree-level barrier between the vacua so that the minimum in the φ axis should be unstable (a saddle point) at zero temperature. We are further interested in a situation in which the critical temperature of this second transition can go parametrically to zero, ensuring a large value of $M_I^0/T_c = y_I \langle \Phi_0 \rangle / T_c$. We consider as an example the case where the metastable and true zero- T vacua are parametrically unrelated: in this case, the energy splitting between them is arbitrary, and in the case where the vacua are nearly degenerate, the temperature at which the intermediate vacuum becomes unstable can be very small. This is the case if the $\Phi \neq 0$ vacuum is aligned with the Φ axis, since the energies of the unstable $(0, v_\varphi)$ and the true $(v_\Phi, 0)$ minimum are determined at tree-level by the independent ratios m_Φ^4/λ_Φ and $m_\varphi^4/\lambda_\varphi$.

To realize this scenario, we study tree-level potentials with an unstable minimum in the φ direction and a stable minimum aligned with the Φ axis, along with a smooth valley of decreasing energy connecting them. This is ensured if the following conditions are satisfied [65, 67]:

$$\frac{m_\varphi^2}{m_\Phi^2} \frac{\lambda_\Phi}{2} \leq \lambda_{\Phi\varphi} \leq \frac{m_\Phi^2}{m_\varphi^2} \frac{\lambda_\varphi}{3}. \quad (66)$$

Being lifted by thermal corrections, the $(v_\Phi, 0)$ “vacuum” has higher energy than that at $(0, v_\varphi)$ at finite temperature. If the vacua are nearly degenerate at $T = 0$, their energies cross at a very small value of T , suggesting that one may achieve large values of M_I^0/T_c . A critical temperature for baryogenesis is that at which the $(0, \varphi)$ vacuum destabilizes and the Majoron Φ can start developing a VEV ($T_c \equiv \tilde{T}_\varphi$). As shown in Section 3.2, a first-order phase transition leads to a suppressed asymmetry, so we consider second-order phase transitions. To avoid energy barriers resulting in a first-order phase transition, \tilde{T}_φ must be larger than the temperature \tilde{T}_Φ at which the $(v_\Phi, 0)$ critical point becomes a stable, local minimum. Using the high-temperature expansion, it can be shown (see Appendix C for details) that the $\tilde{T}_\varphi \rightarrow 0$ limit, together with the condition $\tilde{T}_\varphi > \tilde{T}_\Phi$ for a second-order phase transition between the $(0, v_\varphi)$ and $(v_\Phi, 0)$ minima, is achieved when both of the inequalities in Eq. (66) are saturated. As expected, the temperature \tilde{T}_φ at which the lepton-number-breaking Majoron ϕ acquires a VEV goes to zero parametrically in this degenerate limit.

Crucially, the above arguments do not rely on large Yukawa couplings between N_I and Φ to realize a fast and delayed second-order phase transitions. The conclusions of the previous section, where radiative corrections destroy the stability of the vacuum, therefore do not apply to multi-field models. However, quantum corrections

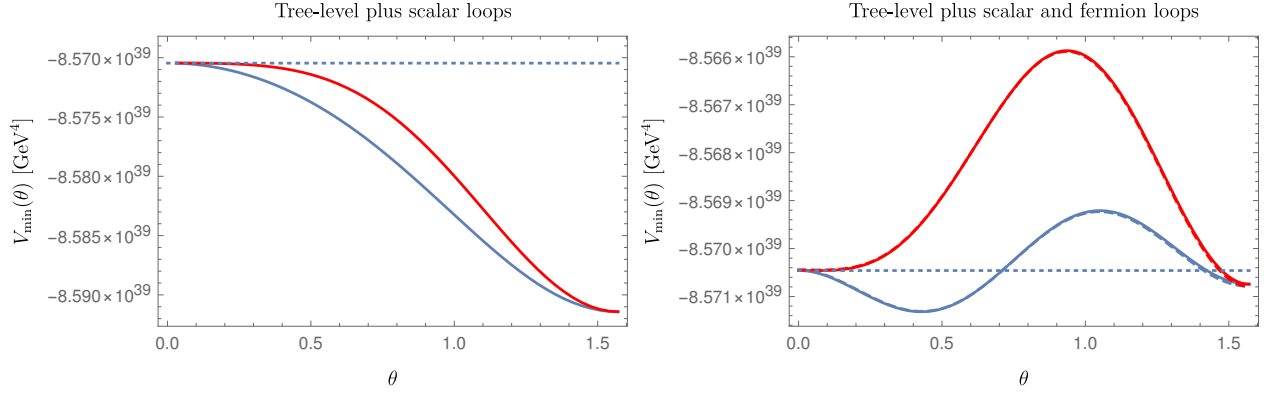


Figure 8: Scalar potential $V_{\min}(\theta)$ along the lowest-energy path connecting the minima along the φ and Φ axes in the two-field symmetry breaking model of Eq. (65). We have parameterized the path with $\theta \equiv \arctan \Phi/\varphi$. On the left, only scalar corrections are included, while the right plot accounts for both scalar and fermion loops. The blue lines have $\lambda_{\Phi\varphi} = 0.07000$, and the red lines $\lambda_{\Phi\varphi} = 0.06994$; the other parameters are specified in the main text. On the right, the solid lines were obtained with a fixed renormalization scale, and the dashed lines with a field-dependent scale set to the maximum of the effective masses in a given Φ, φ background.

can still be important in correctly modelling the phase transition: in the limit where Eq. (66) are saturated, the shape of the potential between them is quite flat at tree level and becomes sensitive to quantum corrections, however small. In particular, such corrections can spoil the existence of a line of decreasing energy connecting the minima. One of two things can occur to spoil the phase transition. First, a zero-temperature barrier may appear, which prevents a second order phase transition and inhibits asymmetry generation for large M_I^0/T_c . Second, a new global minimum with concurrent, nonzero values of Φ and φ might develop. In the latter case, the energy of this minimum stops depends on the energy of the $(0, v_\varphi)$ saddle-point, and consequently the critical temperature of the second phase transition can no longer become parametrically close to zero. Although a second-order phase transition is possible in this case, an upper bound on M_I^0/T_c is obtained.

We examine the effects of radiative corrections on phase transitions in the simplest two-field model, Eq. (65). The quantum corrections arise predominantly due to the Yukawa couplings between Φ and N_I . It is illustrative to consider the path of least energy connecting the minima aligned with each of the Φ and φ axes, which is computed by parameterizing the field space in polar coordinates

$$\varphi = r \cos \theta, \quad \Phi = r \sin \theta, \quad (67)$$

and calculating the energy along the minimal path as

$$V_{\min}(\theta) = \min_r V(r, \theta). \quad (68)$$

Considering only the tree-level potential, we consider parameters in Eq. (65) giving rise to a smooth path of monotonically decreasing energy at zero temperature between the $(0, v_\varphi)$ and $(v_\Phi, 0)$ minima, meaning that $V_{\min}(\theta)$ is a monotonically decreasing function of θ between 0 and π . We then include radiative corrections that may spoil the monotonic behaviour when $V_{\min}(0)$ and $V_{\min}(\pi)$ become sufficiently degenerate. It should be noted that, in our analysis, we do not concern ourselves with issues of fine tuning (which such degeneracies necessarily involve in the absence of a symmetry) and simply ask how radiative corrections would spoil the shape of the potential; we turn later to a discussion on the question of how symmetries may alter this perspective.

We illustrate in Fig. 8 our results for the effects of radiative corrections on the zero-temperature potential, showing the difference between the potential shape when scalar and fermion radiative corrections are added to the potential. We fix $\lambda_\Phi = 0.115475$, $\lambda_\varphi = 0.25400$, $y_1 = 0.33333$, $y_2 = 0.35570$, $m_\Phi^2 = (5.61270 \times 10^9 \text{ GeV})^2$, $m_\varphi^2 = (6.17252 \times 10^9 \text{ GeV})^2$, and either $\lambda_{\Phi\varphi} = 0.07000$ (red curves) or 0.06994 (blue curves). Our calculations show that scalar loops preserve the smooth, monotonic path between vacua, while fermionic interactions either

introduce a barrier or a minimum with non-zero VEVs for both fields (*i.e.*, a global minimum at $\theta \neq 0, \pi$). The appearance of such features is not an artifact of a truncation of perturbation theory, as the theoretical error of the calculations remains much smaller than the size of the features generated by fermionic loops. To show this explicitly, we calculated the potential both with a fixed renormalization scale $\mu = \sqrt{m_\Phi^2}$, or a field-dependent scale $\mu = \max\{m_i(\Phi, \varphi)\}$ set to the maximum of the scalar and fermionic masses in a given (Φ, φ) background. The choice of fixed μ gives the solid lines on the right of Fig. 8, while the field-dependent choice produces the dashed lines.

In the examples shown in Fig. 8, we obtain $M_1^0/T_c \approx 8.3$ for T_c defined as the critical temperature at which the minima in the two field directions become degenerate, and M_1^0 as the field-dependent mass for N_1 in the $(v_\Phi, 0)$ minimum. Potentials with a barrier (such as the red curve in the right pane of Fig. 8) lead to first-order phase transitions and a suppressed baryon asymmetry, and so we must instead consider parameter regimes such as that leading to the blue curve on the right-hand of Fig. 8. In this case, a global minimum occurs with simultaneous non-zero Φ and φ , and as argued above it is not possible to realize a $T_c \rightarrow 0$ limit in this case. Furthermore, the value of Φ at the global minimum is smaller than in the $(v_\Phi, 0)$ configuration: for instance, for the potential with the blue lines in Fig. 8 we get $M_1^0/T_c = 1.7$. It is evident that quantum corrections spoil the region of parameter space that naively realizes a large, parametric enhancement of M_1^0/T_c at leading order. We were unable to find any successful benchmark point in the regime of asymmetry enhancement, (*i.e.*, with $M_{N_1}/T_c \gtrsim 10$) as in Fig. 2.

It is perhaps unsurprising that radiative corrections ruin the parts of parameter space that give rise to delayed phase transitions in tree-level calculations. The level of tuning of parameters is quite high (see, for instance, how a change at the $\sim 10^{-4}$ level in coupling results in the different red and blue curves in Fig. 8), and in the absence of a symmetry, there is no reason that these contributions should cancel. For example, if φ and Φ were embedded in the multiplet of some higher symmetry, then the potential could be exactly flat between the two quasi-minima of the potential. However, the fact that the N_I should only get a mass in the second stage of the phase transition (and therefore only couple appreciably to Φ) resulting in a hard breaking of the symmetry, and leads to the dangerous radiative corrections studied above.

One may consider an alternate possibility, namely that the contribution of the fermionic loops to the scalar potential is cancelled by the contributions of additional scalars with mixed quartic couplings related to the Yukawa couplings, y_I , as in supersymmetric models. In Section 5.1, we found that this introduces a thermal barrier to the new scalar contributions to the effective potential for Φ and φ . This is less of an issue for multi-field models because the barrier height scales with the temperature as in Eq. (63), and so if T_c is parametrically close to zero, the barrier could potentially be irrelevant at $T = T_c$. We have checked that it is indeed possible to get larger values of M_1^0/T_c in the two-field model of Eq. (65) supplemented with two additional scalars. However, when nearing the asymmetry-enhancing regime with $M_1^0/T_c \gtrsim 10$, the required degeneracy between the $(0, v_\varphi)$ saddle-point and the $(v_\Phi, 0)$ minimum becomes comparable to the theoretical uncertainty of the one-loop computation. This results in a strong dependence of the shape of the potential on the choice of the unphysical renormalization scale, which can affect the appearance (or lack thereof) of barriers and other non-trivial features as in Fig. 8. Resolving the issue would require the precision of a two-loop calculation, which is outside the scope of this work but is likely to involve substantial fine-tuning in the model.

We conclude that models with an enhancement of the asymmetry due to a very fast second order phase transition are in principle possible when multi-field transitions are invoked. In the case of two-step transitions, viable models seem to require a carefully arranged particle content with some supersymmetric-like coupling relations, which in the absence of a complete model manifests as a fine tuning. Even still, a definite conclusion requires higher order calculations and presumably a more UV-complete model. Perhaps it is possible to evade the tuning requirements with a larger number of scalar fields and transitions, in which the fields get trapped in a region with zero Φ until very low temperatures are reached; as outlined here, the challenge is to achieve this while guaranteeing a barrier-free path towards the Majoron Φ vacuum at both finite and zero temperature.

6 Conclusions

We have systematically studied the effects of a phase transition on the baryon asymmetry generated via out-of-equilibrium decays. In particular, we have focused on the scenario in which the parent particle responsible for baryogenesis obtains its mass via spontaneous symmetry breaking, and phase transitions in the early universe therefore give rise to a time-dependent mass. This in principle allows for the possibility of an enhanced departure from thermal equilibrium, leading to deviations in the usual predictions for the baryon asymmetry.

The change in the baryon asymmetry due to a time-varying mass for the parent particle depends strongly on the nature of the phase transition. We have found the following:

1. **First-order phase transition:** While an enhancement of the baryon asymmetry due to suppression of washout effects is, in principle, possible with a first-order phase transition, realistic models lead to a reflection of the parent particle at the bubble wall during the phase transition, resulting in an exponential suppression of the asymmetry (see Fig. 1).
2. **Second-order phase transition:** If the mass of the parent particle changes rapidly during the phase transition (*i.e.*, on time scales shorter than the Hubble expansion time), a suppression of baryon-number-violating inverse decays can lead to an enhanced baryon asymmetry. The requirement is that the ratio of the zero temperature mass of the parent relative to the temperature of the phase transition should approximately exceed 10 (see Fig. 2).
3. **Slowly varying mass:** If the mass of the parent particle changes very slowly with time (*i.e.*, on time scales longer than the Hubble expansion time), there is no change in the efficacy of baryogenesis. However, since the mass was different in the early universe relative to today, this changes the relationship among parameters since the time of leptogenesis. In particular, in models of leptogenesis where the right-handed neutrino mass changes slowly with time, then the time scale at which leptogenesis occurs was different in the early universe than would be expected from current neutrino oscillation data. We find that an enhancement of the asymmetry requires larger RH neutrino masses in the early universe, and thus higher reheating temperatures, which is contrary to existing statements in the literature.

With a time-dependent mass due to a varying background scalar field, the asymmetry can also be modified due to annihilations of the parent particle into quanta of the same scalar field. We found that the role of these annihilations is to damp the asymmetry by providing new, baryon-number-conserving modes for depleting the parent abundance. However, the importance of the annihilations depends on the parameters of the model, and they tend to become more important for delayed or fast transitions.

Finally, we considered realistic models of phase transitions driven by the dynamics of single or multiple scalars. We found that obtaining fast and delayed phase transitions, which are necessary to enhance the asymmetry via a second-order phase transition, typically requires large Yukawa couplings that induce radiative corrections spoiling the lateness of the phase transition, or its second-order nature. We discussed possible cancellations among quantum corrections that could lead to a delayed asymmetry tied to a second-order phase transition, concluding that while such phase transitions are possible in principle, they typically rely on some type of fine tuning or the contributions of higher-order corrections that are beyond the scope of this paper. Therefore, we conclude that an enhancement of the asymmetry from out-of-equilibrium decays is unlikely in a generic model, but may be realized in specific UV-complete theories.

Acknowledgements: We are grateful to Peter Ballett, Nikita Blinov, David Morrissey, Michael Peskin, Natalia Toro, Jessica Turner and Ye-Ling Zhou for helpful discussions. BS is supported by the United States Department of Energy under contract DE-AC02-76SF00515.

A CP -Violating Source in the Resonant Regime

In the regime of resonant leptogenesis with near-degenerate N_I , $M_I \sim M_J$ [42, 43], a resummation of self-energy effects is necessary to resolve the $x = 1$ singularity in Eq. (3). For two flavours of N_I particles, the

flavoured CP -sources can be written as [43]

$$\varepsilon_I^\alpha = \frac{1}{8\pi} \frac{1}{(F^\dagger F)_{II}} \sum_{J \neq I} \left\{ \text{Im}[F_{I\alpha}^\dagger F_{\alpha J} (F^\dagger F)_{IJ}] g'(x_{IJ}) \right. \\ \left. + (M_I^2 - M_J^2) \frac{\text{Im} \left[F_{I\alpha}^\dagger F_{\alpha J} (M_I^2 (F^\dagger F)_{JI} + M_I M_J (F^\dagger F)_{IJ}) \right]}{(M_I^2 - M_J^2)^2 + \Delta_{IJ}^2} \right\}. \quad (69)$$

The x_{IJ} are defined in Eq. (3), while the function $g'(x)$ is given by the non-singular part of $g(x)$ in the same equation,

$$g'(x) = \sqrt{x} \left[1 - (1+x) \log \left(\frac{1+x}{x} \right) \right]. \quad (70)$$

The Δ_{IJ} regulate the singularity in the degenerate limit of the sources in Eq. (2), and have been the subject of discussion in the literature; here we choose $\Delta_{12} = \Delta_{21} = M_1 \Gamma_{N_1} + M_2 \Gamma_{N_2}$, which allows the semi-classical Boltzmann equations to better capture coherent quantum effects [68]. In the limit $\Delta_{IJ} \rightarrow 0$, one recovers Eq. (2) from Eq. (69).

B Thermally Averaged Rates

In this Appendix, we establish conventions for our calculations, collecting formulae for the thermally averaged rates. These are constructed from the corresponding reaction densities, which for a process of the form $a + b + \dots \rightarrow i + j + \dots$ are defined as

$$\gamma(a + b + \dots \rightarrow i + j + \dots) \equiv \frac{1}{\mathcal{S}} \int d\Pi_a f_a d\Pi_b f_b \dots |M(a + b + \dots \rightarrow i + j + \dots)|^2 \bar{\delta} d\Pi_i d\Pi_j \dots \quad (71)$$

In the previous equation, we have ignored Bose-enhancement and Pauli-blocking effects, while the squared-matrix element is summed over all external polarizations and \mathcal{S} is a symmetry factor accounting for identical-particle phase-space integration in the initial or final state. $d\Pi_a = d^3 p_a / [(2\pi)^3 2E_a]$, while $\bar{\delta} \equiv (2\pi)^4 \delta^{(4)}(\sum p_a - \sum p_i)$. f_a denote the equilibrium number densities, which we take as given by the Maxwell-Boltzmann distribution with zero chemical potential,

$$f_a(p) = e^{-M_a/T}. \quad (72)$$

For a decay process of a particle N_I , such as the $N_I \rightarrow L_\alpha H$ processes considered in this paper, the thermally averaged decay rate is defined as

$$\langle \Gamma_{N_I} \rangle \equiv \frac{\langle \gamma(N_I \rightarrow \dots) \rangle}{n_{N_I}^{\text{eq}}}, \quad (73)$$

where $n_{N_I}^{\text{eq}}$ is the total equilibrium number density. For a particle a with g_a degrees of freedom,

$$n_a^{\text{eq}} = \frac{g_a}{(2\pi)^3} \int d^3 p f_{N_I}(p) = \frac{g_a T^3}{2\pi^2} \left(\frac{M_a}{T} \right)^2 K_2 \left[\frac{M_a}{T} \right], \quad z^2 K_2[z] = \int_z^\infty x e^{-x} \sqrt{x^2 - z^2}. \quad (74)$$

where the function K_2 behaves asymptotically as

$$z^2 K_2[z] = 2 + \mathcal{O}(z), \quad z^2 K_2[z] = \left(\frac{15}{8} + z \right) \sqrt{\frac{\pi z}{2}} e^{-z} + \mathcal{O}\left(\frac{1}{z}\right). \quad (75)$$

Using Eqs. (71), (73) and (74), for a momentum-independent two-body decay rate such as $\Gamma_{N_I \rightarrow XY}$ (see Eq. (14)) one has

$$\langle \Gamma_{N_I} \rangle = \frac{K_1(z_I)}{K_2(z_I)} \Gamma_{N_I}, \quad z K_1[z] = \int_z^\infty e^{-x} \sqrt{x^2 - z^2}, \quad (76)$$

where $z_I = M_I/T$ and

$$zK_1[z] = 1 + \mathcal{O}(z), \quad zK_1[z] = \sqrt{\frac{\pi z}{2}} e^{-z} + \mathcal{O}\left(\frac{1}{z}\right). \quad (77)$$

Averaged annihilation cross sections for a reaction $N_I + N_I \rightarrow \dots$ are defined as

$$\langle \sigma_{N_I N_I \rightarrow \dots} v \rangle \equiv \frac{\langle \gamma(N_I N_I \rightarrow \dots) \rangle}{(n_{N_I}^{\text{eq}})^2}. \quad (78)$$

Using Eqs. (71) and (74), in the case of a two-body annihilation $N_I N_I \rightarrow XY$ one can write

$$\langle \sigma_{N_I N_I \rightarrow XY} v \rangle = \frac{1}{16T^5 (z_I^2 K_2[z_I])^2} \int ds s^{3/2} K_1 \left[\frac{\sqrt{s}}{T} \right] \left(1 - \frac{4M_I^2}{s} \right) \sigma_{N_I N_I \rightarrow XY}(s), \quad (79)$$

with $\sigma_{N_I N_I \rightarrow XY}(s)$ the usual annihilation cross section averaged over the spins of the N_I , and where we have included an additional factor of $1/2$ for the symmetry factor associated with the initial-state phase-space integration.

C Effective Potential at Zero and Finite Temperature

We give an overview of the construction of the effective potential at finite temperature for a theory with fermions and scalars in the background of scalar fields ϕ_i ; details can be found in many reviews (such as Ref. [69]). At one-loop order, the potential may be expressed as $V = V^0 + V^T$, with V^0 the zero-temperature contribution including one-loop Coleman-Weinberg corrections, and with V^T designating the finite-temperature correction. In the $\overline{\text{MS}}$ scheme, V^0 is given by

$$V^0 = V^{\text{tree}} + \frac{1}{64\pi^2} \left[\sum_S m_S^4(\phi_i) \left(\log \frac{m_S^2(\phi_i)}{\mu^2} - \frac{3}{2} \right) - 2 \sum_F m_F^4(\phi_i) \left(\log \frac{m_F^2(\phi_i)}{\mu^2} - \frac{3}{2} \right) \right], \quad (80)$$

where V^{tree} is the tree-level potential, $m_X(\phi_i)$ is the mass of the field X in a background configuration ϕ_i , and the labels S, F corresponds to scalars and Weyl fermions (the factor of 2 is from each spin contribution for a given Weyl fermion). On the other hand, the one-loop thermal corrections go as

$$V^T = \frac{T^4}{2\pi^2} \left[\sum_B J_B \left(\frac{m_S^2(\phi_i)}{T^2} \right) - 2 \sum_F J_F \left(\frac{m_F^2(\phi_i)}{T^2} \right) \right]. \quad (81)$$

The thermal functions J_S and J_F are given by

$$J_S(x) = \int_0^\infty dy y^2 \log \left[1 - \exp(-\sqrt{x^2 + y^2}) \right], \quad J_F(x) = \int_0^\infty dy y^2 \log \left[1 + \exp(-\sqrt{x^2 + y^2}) \right]. \quad (82)$$

In the large temperature limit, $T \gg m_X(\phi_i)$, the above functions may be approximated as

$$J_S = -\frac{\pi^4}{45} + \frac{\pi^2}{12}x - \frac{\pi}{6}x^{3/2} + \mathcal{O}(x^4), \quad J_F = \frac{7\pi^4}{360} - \frac{\pi^2}{24}x + \mathcal{O}(x^2). \quad (83)$$

The above expansions, together with Eq. (81), imply that the leading effect of a thermal bath is to introduce positive T^2 corrections to the quadratic terms in the potential, stabilizing the scalar fields by enhancing their masses. A single scalar field ϕ undergoes a second-order phase transition if, at some critical temperature T_c , its effective mass crosses zero and becomes negative, triggering the development of a nonzero VEV. The transition remains of the second order as long as no barrier is generated, which happens if the thermal corrections do not generate terms that are cubic in the background fields. Such terms come from the non-analytic $\mathcal{O}(x^{3/2})$ terms in Eq. (83); no ϕ^3 barrier is generated if these contributions are suppressed, or if for the range of interest

of ϕ the bosonic masses that generate the barrier are dominated by their ϕ -independent parts. Whenever ϕ^3 interactions can be neglected, one may use the leading terms to approximate the temperature dependence of the VEV $\langle\phi(T)\rangle$ and the masses of the excitations above the background. This gives the temperature dependence of Eq. (19).

The non-analyticity of $J_S(x)$ for small x in Eq. (83) signals a singular behaviour for zero bosonic masses. In fact, small bosonic masses can be seen to lead to a breakdown of perturbation theory, which can be avoided by resumming thermal corrections to the scalar two-point function [62], a procedure known as ‘‘Daisy resummation’’. Practically, this can be implemented by substituting $m_S^2(\Phi_i)$ in Eq. (81) with the thermally corrected masses.

C.1 Single-Field Model

For the model with interaction as in Eq. (41), consisting of a Majoron field Φ that breaks the baryon number symmetry and gives a mass to right-handed neutrinos N_I , the masses of real scalar fields and Weyl fermions in the background of the Majoron are:

$$m_{S,1}^2 = -m^2 + \frac{\lambda\Phi^2}{2}, \quad m_{S,2}^2 = -m^2 + \frac{3\lambda\Phi^2}{2} \quad m_{F,1} = y_1\Phi, \quad m_{F,2} = y_2\Phi, \quad (84)$$

The one-loop beta functions are, defining $\kappa \equiv (16\pi^2)^{-1}$:

$$\begin{aligned} \beta_\lambda &= \kappa (5\lambda^2 + 2\lambda y_1^2 + 2\lambda y_2^2 - 4y_1^4 - 4y_2^4) + \mathcal{O}(\kappa^2), & \beta_{y_1} &= \frac{\kappa}{2} y_1 (3y_1^2 + y_2^2) + \mathcal{O}(\kappa^2), \\ \beta_{y_2} &= \frac{\kappa}{2} y_2 (y_1^2 + 3y_2^2) + \mathcal{O}(\kappa^2), & \beta_{m^2} &= \kappa m^2 (2\lambda + y_1^2 + y_2^2) + \mathcal{O}(\kappa^2). \end{aligned} \quad (85)$$

The leading thermal corrections induce the following correction to the Majoron mass parameter (with the conventions of Eq. (41)):

$$-m^2 \rightarrow -m^2 + \frac{T^2}{24} \left(2\lambda + \sum_I y_I^2 \right), \quad (86)$$

which gives the following estimate of the critical temperature:

$$T_c^2 = \frac{12\lambda\Phi_0^2}{2\lambda + \sum_I y_I^2}, \quad (87)$$

where Φ_0 is the zero-temperature VEV, $\Phi_0^2 = 2m^2/\lambda$. In the broken phase, the temperature-dependent minimum lies at a VEV given by equation (19) and T_c given in Eq. (87). The masses of scalar excitations around the temperature-dependent minimum, relevant for computing annihilation cross sections as in Section 4, scale as $m_{|\Phi|}^2(T) = \lambda(\Phi(T))^2$ and zero, as Goldstone’s theorem also applies at finite temperature. The field-dependent masses of the N_I are given by Eq. (17).

C.2 Two-Field (N_I - φ -Majoron) Model

This model is characterized by the interactions in Eq. (65). The scalar and fermion masses in an arbitrary Φ, φ background, including the leading finite temperature corrections (as needed for the Daisy resummation)

are given by

$$\begin{aligned}
m_{S,1}^2 &= \frac{1}{24} (12\Phi^2\lambda_\Phi - 24m_\Phi^2 + 12\varphi^2\lambda_{\Phi\varphi}) + \frac{T^2}{24} (2\lambda_\Phi + \lambda_{\Phi\varphi} + y_1^2 + y_2^2), \\
m_{S,2}^2 &= \frac{1}{48} \left\{ 24\Phi^2\lambda_{\Phi\varphi} + 36\Phi^2\lambda_\Phi - \left[(36\Phi^2\lambda_\Phi - 24m_\varphi^2 - 24m_\Phi^2 + 12\varphi^2(\lambda_{\Phi\varphi} + \lambda_\varphi) + T^2\lambda_\varphi + 3\lambda_{\Phi\varphi}(T^2 + 8\Phi^2) \right. \right. \\
&\quad + 2T^2\lambda_\Phi + T^2y_1^2 + T^2y_2^2)^2 - 4((12\varphi^2 + T^2)\lambda_\varphi - 24m_\varphi^2)(-24m_\Phi^2 + 2\lambda_\Phi(T^2 + 18\Phi^2) + T^2(y_1^2 + y_2^2)) \\
&\quad - 4\lambda_{\Phi\varphi}(-24m_\varphi^2(12\varphi^2 + T^2) - 48m_\Phi^2(T^2 + 12\Phi^2) + 144\varphi^4\lambda_\varphi + T^2((24\varphi^2 + T^2)\lambda_\varphi \\
&\quad + 2(y_1^2 + y_2^2)(T^2 + 12\Phi^2)) + 4\lambda_\Phi(T^4 + 30T^2\Phi^2 + 216\Phi^4)) - 8\lambda_{\Phi\varphi}^2(12\varphi^2(T^2 - 36\Phi^2) \\
&\quad \left. \left. + T^4 + 12T^2\Phi^2) \right]^{1/2} - 24m_\varphi^2 - 24m_\Phi^2 + 12\varphi^2\lambda_{\Phi\varphi} + 12\varphi^2\lambda_\varphi \right\} + \frac{T^2}{48} (2\lambda_\Phi + 3\lambda_{\Phi\varphi} + \lambda_\varphi + y_1^2 + y_2^2), \\
m_{S,3}^2 &= \frac{1}{48} \left\{ 24\Phi^2\lambda_{\Phi\varphi} + 36\Phi^2\lambda_\Phi + \left[(36\Phi^2\lambda_\Phi - 24m_\varphi^2 - 24m_\Phi^2 + 12\varphi^2(\lambda_{\Phi\varphi} + \lambda_\varphi) + T^2\lambda_\varphi + 3\lambda_{\Phi\varphi}(T^2 + 8\Phi^2) \right. \right. \\
&\quad + 2T^2\lambda_\Phi + T^2y_1^2 + T^2y_2^2)^2 - 4((12\varphi^2 + T^2)\lambda_\varphi - 24m_\varphi^2)(-24m_\Phi^2 + 2\lambda_\Phi(T^2 + 18\Phi^2) + T^2(y_1^2 + y_2^2)) \\
&\quad - 4\lambda_{\Phi\varphi}(-24m_\varphi^2(12\varphi^2 + T^2) - 48m_\Phi^2(T^2 + 12\Phi^2) + 144\varphi^4\lambda_\varphi + T^2((24\varphi^2 + T^2)\lambda_\varphi \\
&\quad + 2(y_1^2 + y_2^2)(T^2 + 12\Phi^2)) + 4\lambda_\Phi(T^4 + 30T^2\Phi^2 + 216\Phi^4)) - 8\lambda_{\Phi\varphi}^2(12\varphi^2(T^2 - 36\Phi^2) + T^4 \\
&\quad \left. \left. + 12T^2\Phi^2) \right]^{1/2} - 24m_\varphi^2 - 24m_\Phi^2 + 12\varphi^2\lambda_{\Phi\varphi} + 12\varphi^2\lambda_\varphi \right\} + \frac{T^2}{48} (2\lambda_\Phi + 3\lambda_{\Phi\varphi} + \lambda_\varphi + y_1^2 + y_2^2). \tag{88}
\end{aligned}$$

The one-loop beta functions (used to implement the one-loop potential with a field-dependent renormalization scale) are in this case

$$\begin{aligned}
\beta_{\lambda_\Phi} &= \kappa (5\lambda_\Phi^2 + 2\lambda_{\Phi\varphi}^2 + 2\lambda_\Phi(y_1^2 + y_2^2) - 4y_1^4 - 4y_2^4) + \mathcal{O}(\kappa^2), & \beta_{\lambda_\varphi} &= 3\kappa (\lambda_\varphi^2 + 2\lambda_{\Phi\varphi}^2) + \mathcal{O}(\kappa^2), \\
\beta_{\lambda_{\Phi\varphi}} &= \kappa\lambda_{\Phi\varphi} (\lambda_\varphi + 2\lambda_\Phi + 4\lambda_{\Phi\varphi} + y_1^2 + y_2^2) + \mathcal{O}(\kappa^2), & \beta_{y_1} &= \frac{\kappa}{2}y_1 (3y_1^2 + y_2^2) + \mathcal{O}(\kappa^2), \\
\beta_{m_\Phi^2} &= \kappa (\lambda_{\Phi\varphi}m_\varphi^2 + m_\Phi^2(2\lambda_\Phi + y_1^2 + y_2^2)) + \mathcal{O}(\kappa^2), & \beta_{y_2} &= \frac{\kappa}{2}y_2 (y_1^2 + 3y_2^2) + \mathcal{O}(\kappa^2), \\
\beta_{m_\varphi^2} &= \kappa (\lambda_\varphi m_\varphi^2 + 2\lambda_{\Phi\varphi}m_\Phi^2) + \mathcal{O}(\kappa^2).
\end{aligned} \tag{89}$$

The temperature-induced mass corrections in the high-temperature approximation are:

$$-m_\Phi^2 \rightarrow -m_\Phi^2 + \frac{T^2}{24} \left(2\lambda_\Phi + \sum_I y_I^2 + \xi \right), \quad -m_\varphi^2 \rightarrow -m_\varphi^2 + \frac{T^2}{24} (\lambda_S + 2\xi). \tag{90}$$

As elaborated in the main text, we are interested in scenarios in which at high temperatures there exists a vacuum in the $(0, \varphi)$ direction, which becomes unstable at lower temperatures and gives rise to a second-order phase transition to the $(\Phi, 0)$ minimum. During the phase transition, the minimum moves from one field direction to the other without encountering any barrier. The fact that such scenarios are, in principle, feasible can be seen with the tree-level potential plus the dominant T^2 corrections to the mass parameters (the T^4 terms are field-independent and thus do not affect phase transitions). One may define the following temperatures:

- T_φ : Temperature at which a minimum degenerate with the origin appears in the $(0, \varphi)$ direction.
- T_Φ : Temperature at which a minimum degenerate with the origin appears in the $(\Phi, 0)$ direction.
- \tilde{T}_φ : Temperature at which the minimum in the $(0, \varphi)$ direction becomes unstable.

- \tilde{T}_Φ : Temperature at which the minimum in the $(\Phi, 0)$ direction becomes stable.

In the scenarios of interest, we want first a transition to a $(0, v_\varphi)$ vacuum, which should become unstable before the $(v_\Phi, 0)$ minimum in the Φ axis is stabilized, as otherwise the latter would lie behind an energy barrier. This means $T_\varphi > T_\Phi > \tilde{T}_\varphi > \tilde{T}_\Phi$. In this case \tilde{T}_φ will be the critical temperature at which the Majoron starts acquiring a VEV in a second-order phase transition, and in scenarios with an enhanced asymmetry we want to ensure $M_{N_I}/\tilde{T}_\varphi = y_I \langle \Phi \rangle / \tilde{T}_\varphi \gg 1$. Parametrizing mass scales in terms of the zero-temperature VEVs of the minima aligned with the field directions,

$$\langle \Phi \rangle^2 \equiv \frac{2m_\Phi^2}{\lambda_\Phi}, \quad \langle \varphi \rangle^2 \equiv \frac{6m_\varphi^2}{\lambda_\varphi}, \quad (91)$$

then in these approximations the previously defined temperatures are given by:

$$\begin{aligned} T_\varphi^2 &= \frac{4\lambda_\varphi \langle \varphi \rangle^2}{\lambda_\varphi + 2\xi}, & T_\Phi^2 &= \frac{12\lambda_\Phi \langle \Phi \rangle^2}{2\lambda_\Phi + \xi + \tilde{y}^2}, \\ \tilde{T}_\varphi^2 &= \frac{12\lambda_\varphi (\lambda_\Phi \langle \Phi \rangle^2 - \xi \langle \varphi \rangle^2)}{2\lambda_\Phi \lambda_\varphi - 6\xi^2 + \lambda_\varphi (\tilde{y}^2 - 2\xi)}, & \tilde{T}_\Phi^2 &= \frac{4\lambda_\Phi (6\xi \langle \Phi \rangle^2 - \lambda_\varphi \langle \varphi \rangle^2)}{2\xi (\xi + \tilde{y}^2) - \lambda_\Phi (\lambda_\varphi - 2\xi)}, \end{aligned} \quad (92)$$

where we defined $\tilde{y}^2 \equiv \sum_I y_I^2$. In the scenarios of interest with $\tilde{T}_\varphi > \tilde{T}_\Phi$, and furthermore $\tilde{T}_\varphi \rightarrow 0$ in order to get an enhancement of the asymmetry, one has

$$\lambda_\Phi - \xi \frac{\langle \varphi \rangle^2}{\langle \Phi \rangle^2} \gtrsim 0, \quad \lambda_\varphi - 6\xi \frac{\langle \Phi \rangle^2}{\langle \varphi \rangle^2} \lesssim 0, \quad (93)$$

which by virtue of equation (91) enforces the same inequalities as the conditions Eq. (66) ensuring the absence of a barrier at zero temperature. Within this tree-level, high-temperature expansion, the transition from the $(0, v_\varphi)$ to the (v_Φ) minimum is indeed second-order, and one may follow how the minimum moves from the φ to the Φ axis as a function of temperature. For $\tilde{T}_\varphi > T > \tilde{T}_\Phi$, the minimum lies in between the two field directions, and then settles on the Φ axis for $T \leq \tilde{T}_\Phi$:

$$\left. \begin{aligned} \langle \varphi \rangle^2(T) &= \frac{(T^2 - \tilde{T}_\Phi^2)(2\xi(\xi + \tilde{y}_X^2) - \lambda_\Phi(\lambda_\varphi - 2\xi))}{4(\lambda_\Phi \lambda_\varphi - 6\xi^2)} \\ \langle \Phi \rangle^2(T) &= \frac{(\tilde{T}_\varphi^2 - T^2)(2\lambda_\Phi \lambda_\varphi - 6\xi^2 + \lambda_\varphi(\tilde{y}_X^2 - 2\xi))}{12(\lambda_\Phi \lambda_\varphi - 6\xi^2)} \end{aligned} \right\} \quad \tilde{T}_s \geq T \geq \tilde{T}_\Phi. \quad (94)$$

$$\left. \begin{aligned} \langle \varphi \rangle^2(T) &= 0 \\ \langle \Phi \rangle^2(T) &= \frac{(T_\Phi^2 - T^2)\langle \Phi \rangle^2}{T_\Phi^2} \end{aligned} \right\} \quad \tilde{T} < \tilde{T}_\Phi. \quad (95)$$

D Annihilation Cross Sections

In this section we consider the annihilation cross sections of N_I particles into the components of a complex Majoron field Φ , in a model with the interactions of Eq. (41), distinguishing the broken and unbroken symmetry cases. The cross sections are averaged over the spins of the initial particles.

D.1 Broken phase

We will assume that the field Φ acquires a background value, which will be assumed to affect its real part; for a CP -invariant evolution of Φ , this can be ensured with an appropriate rotation of the field. In order to calculate annihilations of N_I into the degrees of freedom in Φ , we redefine the latter as

$$\Phi = \frac{1}{\sqrt{2}}(v_\phi + \phi_r)e^{i\phi_i/v_\phi}, \quad (96)$$

where v_ϕ parameterizes the background. The field ϕ_i can be interpreted as the (pseudo-)Goldstone of the (approximate) symmetry that forbids the tree-level mass term for the N_I . The N_I fields can be redefined to absorb the ϕ_i phase, which appears then only in the kinetic terms. The annihilation $NN \rightarrow \phi_r \phi_r$ scalars proceeds through diagrams as in Fig. 4. The interactions in Eq. (41) generate a cubic term for ϕ_r of the form $\mathcal{L} \supset \kappa/6\phi_r^3$, with $\kappa = 3\lambda_\phi v_\phi/2$. The annihilation rate is then given in terms of the masses M and m of the N_I particles and ϕ_r in the v_ϕ background as:

$$\begin{aligned} \sigma_{N_I N_I \rightarrow \phi_r \phi_r}(s) = & \frac{1}{64\pi s(s-4M^2)} \left\{ \sqrt{s-4m^2} \sqrt{s-4M^2} \left[\frac{\kappa^2 (s-4M^2)}{m^2 \Gamma_\phi^2 + (m^2-s)^2} + \frac{8\kappa M y_I (m^2-s)}{m^2 \Gamma_\phi^2 + (m^2-s)^2} \right. \right. \\ & - 4y_I^2 \left(M^4 \left(\frac{4}{m^4 + 2m^2(s-2M^2) + M^2 s} + \frac{4}{m^4 - 4m^2 M^2 + M^2 s} \right) + 1 \right) \Big] \\ & + \frac{y_I}{s(m^2 \Gamma_\phi^2 + (m^2-s)^2)} [2\kappa M s (m^2-s)(s-8M^2) + y_I (s^2 + 16M^2 s - 32M^4) (m^2 \Gamma_\phi^2 \\ & + (m^2-s)^2)] \left[\log \left(m^2 - \frac{1}{2} \sqrt{s-4m^2} \sqrt{s-4M^2} - \frac{s}{2} \right) \right. \\ & \left. \left. - \log \left(m^2 + \frac{1}{2} \sqrt{s-4m^2} \sqrt{s-4M^2} - \frac{s}{2} \right) + 2 \coth^{-1} \left(\frac{2m^2+s}{\sqrt{s-4m^2} \sqrt{s-4M^2}} \right) \right] \right\}. \end{aligned} \quad (97)$$

In the above equation, s is the centre-of-mass energy, and we allowed for a scalar width Γ_ϕ .

For the annihilation cross section into ϕ_i , whose mass is taken as negligible as would be expected for a (pseudo-)Goldstone boson, the process arises again from diagrams as in Fig. 4 but with vertices involving derivative interactions. The result is:

$$\begin{aligned} \sigma_{N_I N_I \rightarrow \phi_i \phi_i}(s) = & \frac{y_I^4}{256\pi M^2 (4M^2-s) (m^2 \Gamma_\phi^2 + (m^2-s)^2)} \left\{ -m^4 \sqrt{s(s-4M^2)} - m^2 \Gamma_\phi^2 \sqrt{s(s-4M^2)} \right. \\ & + M^2 (m^4 + m^2 \Gamma_\phi^2 - s^2) \left[\log \left(-\sqrt{s-4M^2} - \sqrt{s} \right) - \log \left(\sqrt{s-4M^2} - \sqrt{s} \right) \right. \\ & \left. \left. + 2 \tanh^{-1} \left(\sqrt{1 - \frac{4M^2}{s}} \right) \right] + 4M^2 s^{3/2} \sqrt{s-4M^2} \right\}. \end{aligned} \quad (98)$$

D.2 Unbroken phase

In this case the complex Majoron field creates and destroys particles and antiparticles with equal mass. In the absence of a Majoron background there is no induced cubic term in the potential, and so contributing diagrams are as in the left pane of Fig. 4 with $\Phi\Phi^*$ final states. The chiral symmetry under which both N_I and Φ are charged forbids a tree-level mass for the N_I and is not broken by thermal effects. The total annihilation cross section is (for scalar mass m),

$$\sigma_{N_I N_I \rightarrow \Phi\Phi^*}(s) = \frac{y_I^4}{32\pi s^2} \left\{ (s-2m^2) \log \left[\frac{2m^2-s-\sqrt{s(s-4m^2)}}{2m^2-s+\sqrt{s(s-4m^2)}} \right] - 2\sqrt{s(s-4m^2)} \right\}. \quad (99)$$

E Select Yukawa Matrices Used in Calculations

To facilitate reproducing our results, in this appendix we display some of the randomly generated Yukawa matrices used for the calculations leading to Figures 1, 2, 3, and 5.

Figure 1

$$F = \begin{bmatrix} 0.0044448 - 0.00781103i, & -0.000585946 + 0.000711637i \\ 0.00166355 - 0.00412115i, & -0.0066961 + 0.00202516i \end{bmatrix}. \quad (100)$$

Figure 2

Solid line

$$F = \begin{bmatrix} 0.00102987 - 0.000114246i, & -0.000879321 - 0.000112016i \\ 0.000618558 - 0.000648136i, & -0.000791007 + 0.00036227i \\ -0.000449793 - 0.00057956i, & -0.000622262 - 0.000912736i \end{bmatrix}. \quad (101)$$

Dashed line

$$F = \begin{bmatrix} -0.000352184 + 0.000335879i, & -0.000909679 + 0.000368808i \\ 0.000890837 + 0.000306683i, & -0.000782095 + 0.000198108i \\ -0.000548051 + 0.000624317i, & 0.00114164 + 0.0000493831i \end{bmatrix}. \quad (102)$$

Figure 3

Same as Eq. (101).

Figure 5

As detailed in the text, our choice of Yukawa matrices is based upon a reference matrix F_7 :

$$F_7 = \begin{bmatrix} 3.24445 \times 10^{-5} - 5.02185 \times 10^{-6}i, & -9.59362 \times 10^{-5} - 5.89939 \times 10^{-5}i \\ -8.48425 \times 10^{-5} + 9.00147 \times 10^{-5}i, & 3.17704 \times 10^{-5} - 4.27856 \times 10^{-5}i \\ -5.78330 \times 10^{-6} - 7.16867 \times 10^{-5}i, & -3.99969 \times 10^{-6} - 1.87141 \times 10^{-5}i \end{bmatrix}. \quad (103)$$

Figure 6

The left plot uses the Yukawa matrix of Eq. (103), while the right plot uses Eq. (101).

References

- [1] S. L. Glashow, *Partial Symmetries of Weak Interactions*, *Nucl. Phys.* **22** (1961) 579–588.
- [2] S. Weinberg, *A Model of Leptons*, *Phys. Rev. Lett.* **19** (1967) 1264–1266.
- [3] A. Salam, *Weak and Electromagnetic Interactions*, *Conf. Proc.* **C680519** (1968) 367–377.
- [4] SLD ELECTROWEAK GROUP, DELPHI, ALEPH, SLD, SLD HEAVY FLAVOUR GROUP, OPAL, LEP ELECTROWEAK WORKING GROUP, L3 collaboration, S. Schael et al., *Precision electroweak measurements on the Z resonance*, *Phys. Rept.* **427** (2006) 257–454, [[hep-ex/0509008](#)].
- [5] The ALEPH, DELPHI, L3, OPAL Collaborations, the LEP Electroweak Working Group, *Electroweak Measurements in Electron-Positron Collisions at W-Boson-Pair Energies at LEP*, *Phys. Rept.* **532** (2013) 119, [[1302.3415](#)].

- [6] ATLAS collaboration, G. Aad et al., *Observation of a new particle in the search for the Standard Model Higgs boson with the ATLAS detector at the LHC*, *Phys. Lett.* **B716** (2012) 1–29, [1207.7214].
- [7] CMS collaboration, S. Chatrchyan et al., *Observation of a new boson at a mass of 125 GeV with the CMS experiment at the LHC*, *Phys. Lett.* **B716** (2012) 30–61, [1207.7235].
- [8] D. A. Kirzhnits, *Weinberg model in the hot universe*, *JETP Lett.* **15** (1972) 529–531.
- [9] L. Dolan and R. Jackiw, *Symmetry Behavior at Finite Temperature*, *Phys. Rev.* **D9** (1974) 3320–3341.
- [10] S. Weinberg, *Gauge and Global Symmetries at High Temperature*, *Phys. Rev.* **D9** (1974) 3357–3378.
- [11] A. D. Sakharov, *Violation of CP Invariance, c Asymmetry, and Baryon Asymmetry of the Universe*, *Pisma Zh. Eksp. Teor. Fiz.* **5** (1967) 32–35.
- [12] V. A. Kuzmin, V. A. Rubakov and M. E. Shaposhnikov, *On the Anomalous Electroweak Baryon Number Nonconservation in the Early Universe*, *Phys. Lett.* **B155** (1985) 36.
- [13] M. E. Shaposhnikov, *Possible Appearance of the Baryon Asymmetry of the Universe in an Electroweak Theory*, *JETP Lett.* **44** (1986) 465–468.
- [14] M. E. Shaposhnikov, *Baryon Asymmetry of the Universe in Standard Electroweak Theory*, *Nucl. Phys.* **B287** (1987) 757–775.
- [15] A. I. Bochkarev and M. E. Shaposhnikov, *Electroweak Production of Baryon Asymmetry and Upper Bounds on the Higgs and Top Masses*, *Mod. Phys. Lett.* **A2** (1987) 417.
- [16] K. Kajantie, M. Laine, K. Rummukainen and M. E. Shaposhnikov, *Is there a hot electroweak phase transition at $m(H)$ larger or equal to $m(W)$?*, *Phys. Rev. Lett.* **77** (1996) 2887–2890, [hep-ph/9605288].
- [17] D. E. Morrissey and M. J. Ramsey-Musolf, *Electroweak baryogenesis*, *New J. Phys.* **14** (2012) 125003, [1206.2942].
- [18] S. Weinberg, *Cosmological Production of Baryons*, *Phys. Rev. Lett.* **42** (1979) 850–853.
- [19] M. Fukugita and T. Yanagida, *Baryogenesis Without Grand Unification*, *Phys. Lett.* **B174** (1986) 45–47.
- [20] P. Minkowski, *$\mu \rightarrow e\gamma$ at a Rate of One Out of 10^9 Muon Decays?*, *Phys. Lett.* **B67** (1977) 421–428.
- [21] M. Yoshimura, *Unified Gauge Theories and the Baryon Number of the Universe*, *Phys. Rev. Lett.* **41** (1978) 281–284.
- [22] A. Yu. Ignatiev, N. V. Krasnikov, V. A. Kuzmin and A. N. Tavkhelidze, *Universal CP Noninvariant Superweak Interaction and Baryon Asymmetry of the Universe*, *Phys. Lett.* **B76** (1978) 436–438.
- [23] V. V. Khoze and A. D. Plascencia, *Dark Matter and Leptogenesis Linked by Classical Scale Invariance*, *JHEP* **11** (2016) 025, [1605.06834].
- [24] R. N. Mohapatra, *Mechanism for Understanding Small Neutrino Mass in Superstring Theories*, *Phys. Rev. Lett.* **56** (1986) 561–563.
- [25] R. N. Mohapatra and J. W. F. Valle, *Neutrino Mass and Baryon Number Nonconservation in Superstring Models*, *Phys. Rev.* **D34** (1986) 1642.
- [26] A. Pilaftsis and T. E. J. Underwood, *Electroweak-scale resonant leptogenesis*, *Phys. Rev.* **D72** (2005) 113001, [hep-ph/0506107].
- [27] A. Pilaftsis, *Electroweak Resonant Leptogenesis in the Singlet Majoron Model*, *Phys. Rev.* **D78** (2008) 013008, [0805.1677].

- [28] P.-H. Gu and U. Sarkar, *Leptogenesis Bound on Spontaneous Symmetry Breaking of Global Lepton Number*, *Eur. Phys. J.* **C71** (2011) 1560, [0909.5468].
- [29] D. Aristizabal Sierra, M. Tortola, J. W. F. Valle and A. Vicente, *Leptogenesis with a dynamical seesaw scale*, *JCAP* **1407** (2014) 052, [1405.4706].
- [30] A. Ganguly, J. C. Parikh and U. Sarkar, *Low-energy leptogenesis in left-right symmetric models*, *Phys. Lett.* **B385** (1996) 175–180, [hep-ph/9408271].
- [31] L. D. McLerran, M. E. Shaposhnikov, N. Turok and M. B. Voloshin, *Why the baryon asymmetry of the universe is approximately 10^{-10}* , *Phys. Lett.* **B256** (1991) 451–456.
- [32] X.-J. Bi, P.-h. Gu, X.-l. Wang and X.-m. Zhang, *Thermal leptogenesis in a model with mass varying neutrinos*, *Phys. Rev.* **D69** (2004) 113007, [hep-ph/0311022].
- [33] S. Pascoli, J. Turner and Y.-L. Zhou, *Baryogenesis via leptonic CP-violating phase transition*, 1609.07969.
- [34] A. G. Cohen, D. B. Kaplan and A. E. Nelson, *Baryogenesis at the weak phase transition*, *Nucl. Phys.* **B349** (1991) 727–742.
- [35] B. Fornal, Y. Shirman, T. M. P. Tait and J. R. West, *Asymmetric Dark Matter and Baryogenesis from $SU(2)$ -Lepton*, 1703.00199.
- [36] A. J. Long, A. Tesi and L.-T. Wang, *Baryogenesis at a Lepton-Number-Breaking Phase Transition*, 1703.04902.
- [37] A. Katz and A. Riotto, *Baryogenesis and Gravitational Waves from Runaway Bubble Collisions*, *JCAP* **1611** (2016) 011, [1608.00583].
- [38] T. Cohen, D. E. Morrissey and A. Pierce, *Changes in Dark Matter Properties After Freeze-Out*, *Phys. Rev.* **D78** (2008) 111701, [0808.3994].
- [39] I. Baldes, T. Konstandin and G. Servant, *A First-Order Electroweak Phase Transition in the Standard Model from Varying Yukawas*, 1604.04526.
- [40] S. Davidson, E. Nardi and Y. Nir, *Leptogenesis*, *Phys. Rept.* **466** (2008) 105–177, [0802.2962].
- [41] L. Covi, E. Roulet and F. Vissani, *CP violating decays in leptogenesis scenarios*, *Phys. Lett.* **B384** (1996) 169–174, [hep-ph/9605319].
- [42] A. Pilaftsis, *CP violation and baryogenesis due to heavy Majorana neutrinos*, *Phys. Rev.* **D56** (1997) 5431–5451, [hep-ph/9707235].
- [43] A. Pilaftsis and T. E. J. Underwood, *Resonant leptogenesis*, *Nucl. Phys.* **B692** (2004) 303–345, [hep-ph/0309342].
- [44] E. W. Kolb and M. S. Turner, *The Early Universe*, *Front. Phys.* **69** (1990) 1–547.
- [45] A. Abada, S. Davidson, A. Ibarra, F. X. Josse-Michaux, M. Losada and A. Riotto, *Flavour Matters in Leptogenesis*, *JHEP* **09** (2006) 010, [hep-ph/0605281].
- [46] P. Gu, X. Wang and X. Zhang, *Dark energy and neutrino mass limits from baryogenesis*, *Phys. Rev.* **D68** (2003) 087301, [hep-ph/0307148].
- [47] W. Buchmüller and S. Fredenhagen, *Quantum mechanics of baryogenesis*, *Phys. Lett.* **B483** (2000) 217–224, [hep-ph/0004145].

- [48] A. De Simone and A. Riotto, *Quantum Boltzmann Equations and Leptogenesis*, *JCAP* **0708** (2007) 002, [[hep-ph/0703175](#)].
- [49] A. E. Nelson, D. B. Kaplan and A. G. Cohen, *Why there is something rather than nothing: Matter from weak interactions*, *Nucl. Phys.* **B373** (1992) 453–478.
- [50] M.-z. Li, X.-l. Wang, B. Feng and X.-m. Zhang, *Quintessence and spontaneous leptogenesis*, *Phys. Rev.* **D65** (2002) 103511, [[hep-ph/0112069](#)].
- [51] PLANCK collaboration, P. A. R. Ade et al., *Planck 2015 results. XIII. Cosmological parameters*, *Astron. Astrophys.* **594** (2016) A13, [[1502.01589](#)].
- [52] S. Davidson and A. Ibarra, *A Lower bound on the right-handed neutrino mass from leptogenesis*, *Phys. Lett.* **B535** (2002) 25–32, [[hep-ph/0202239](#)].
- [53] J. R. Ellis, J. E. Kim and D. V. Nanopoulos, *Cosmological Gravitino Regeneration and Decay*, *Phys. Lett.* **B145** (1984) 181–186.
- [54] I. Esteban, M. C. Gonzalez-Garcia, M. Maltoni, I. Martinez-Soler and T. Schwetz, *Updated fit to three neutrino mixing: exploring the accelerator-reactor complementarity*, *JHEP* **01** (2017) 087, [[1611.01514](#)].
- [55] J. A. Casas and A. Ibarra, *Oscillating neutrinos and muon $\rightarrow e$, gamma*, *Nucl. Phys.* **B618** (2001) 171–204, [[hep-ph/0103065](#)].
- [56] G. Degrandi, S. Di Vita, J. Elias-Miro, J. R. Espinosa, G. F. Giudice, G. Isidori et al., *Higgs mass and vacuum stability in the Standard Model at NNLO*, *JHEP* **08** (2012) 098, [[1205.6497](#)].
- [57] D. Buttazzo, G. Degrandi, P. P. Giardinò, G. F. Giudice, F. Sala, A. Salvio et al., *Investigating the near-criticality of the Higgs boson*, *JHEP* **12** (2013) 089, [[1307.3536](#)].
- [58] D. Metaxas and E. J. Weinberg, *Gauge independence of the bubble nucleation rate in theories with radiative symmetry breaking*, *Phys. Rev.* **D53** (1996) 836–843, [[hep-ph/9507381](#)].
- [59] A. D. Plascencia and C. Tamarit, *Convexity, gauge-dependence and tunneling rates*, *JHEP* **10** (2016) 099, [[1510.07613](#)].
- [60] C. Ford, D. R. T. Jones, P. W. Stephenson and M. B. Einhorn, *The Effective potential and the renormalization group*, *Nucl. Phys.* **B395** (1993) 17–34, [[hep-lat/9210033](#)].
- [61] J. R. Espinosa, G. F. Giudice and A. Riotto, *Cosmological implications of the Higgs mass measurement*, *JCAP* **0805** (2008) 002, [[0710.2484](#)].
- [62] R. D. Pisarski, *Scattering Amplitudes in Hot Gauge Theories*, *Phys. Rev. Lett.* **63** (1989) 1129.
- [63] D. Land and E. D. Carlson, *Two stage phase transition in two Higgs models*, *Phys. Lett.* **B292** (1992) 107–112, [[hep-ph/9208227](#)].
- [64] A. Hammerschmitt, J. Kripfganz and M. G. Schmidt, *Baryon asymmetry from a two stage electroweak phase transition?*, *Z. Phys.* **C64** (1994) 105–110, [[hep-ph/9404272](#)].
- [65] Y. Cui, L. Randall and B. Shuve, *Emergent Dark Matter, Baryon, and Lepton Numbers*, *JHEP* **08** (2011) 073, [[1106.4834](#)].
- [66] H. H. Patel and M. J. Ramsey-Musolf, *Stepping Into Electroweak Symmetry Breaking: Phase Transitions and Higgs Phenomenology*, *Phys. Rev.* **D88** (2013) 035013, [[1212.5652](#)].
- [67] N. Blinov, J. Kozaczuk, D. E. Morrissey and C. Tamarit, *Electroweak Baryogenesis from Exotic Electroweak Symmetry Breaking*, *Phys. Rev.* **D92** (2015) 035012, [[1504.05195](#)].

- [68] M. Garry, A. Kartavtsev and A. Hohenegger, *Leptogenesis from first principles in the resonant regime*, *Annals Phys.* **328** (2013) 26–63, [1112.6428].
- [69] M. Quiros, *Finite temperature field theory and phase transitions*, in *Proceedings, Summer School in High-energy physics and cosmology: Trieste, Italy, June 29-July 17, 1998*, pp. 187–259, 1999. hep-ph/9901312.